# A global perspective on $CO_2$ satellite observations in high AOD conditions

Timo H. Virtanen[1], Anu-Maija Sundström[2], Elli Suhonen[2], Antti Lipponen[1], Antti Arola[1], Christopher O'Dell[3], Robert R. Nelson[4], and Hannakaisa Lindqvist[2]

[1]Finnish Meteorological Institute, Climate Research Programme, Helsinki, Finland
[2]Finnish Meteorological Institute, Space and Earth Observation Centre, Helsinki, Finland
[3]Colorado State University, Fort Collins, CO, USA
[4]Jet Propulsion Laboratory, California Institute of Technology, CA USA

**Correspondence:** Timo H. Virtanen (timo.h.virtanen@fmi.fi)

**Abstract.** Satellite-based observations of carbon dioxide ($CO_2$) are sensitive to all processes that affect the propagation of radiation in the atmosphere, including scattering and absorption by atmospheric aerosols. Therefore, accurate retrievals of column-averaged $CO_2$ ($XCO_2$) benefit from detailed information on the aerosol conditions. This is particularly relevant for future missions focusing on observing anthropogenic $CO_2$ emissions, such as the Copernicus Anthropogenic $CO_2$ Monitoring mission (CO2M). To fully prepare for CO2M observations, it is informative to investigate existing observations in addition to other approaches. Our focus here is on observations from the NASA Orbiting Carbon Observatory -2 (OCO-2) mission. In the operational full-physics $XCO_2$ retrieval used to generate OCO-2 level 2 products, the aerosol properties are known to have high uncertainty but their main objective is to facilitate $CO_2$ retrievals. We evaluate the OCO-2 product from the point of view of aerosols by comparing the OCO-2 retrieved aerosol properties to collocated Moderate Resolution Imaging Spectro-radiometer (MODIS) Aqua Dark Target aerosol products. We find that there is a systematic difference between the aerosol optical depth (AOD, $\tau$) values retrieved by the two instruments, such that $\tau_{\mathrm{OCO-2}} \sim 0.4\tau_{\mathrm{MODIS}}$. Similar difference is found when comparing OCO-2 with the Aerosol Robotic Network (AERONET). This results in 16.5% of cases being misclassified as low AOD (good quality) by the OCO-2 quality filtering. We also find a dependence of the $XCO_2$ on the AOD difference, indicating an aerosol-induced effect in the $XCO_2$ retrieval. Furthermore, comparing with Total Carbon Column Observing Network (TCCON), we find a small AOD dependent bias in $XCO_2$. In addition, we find a weak but statistically significant correlation between MODIS AOD and $XCO_2$, which can be partly explained by natural covariance and co-emission of aerosols and $CO_2$. Due to the co-emission, using an AOD threshold in the quality filtering leads to a sampling bias, where high $XCO_2$ values are more often removed. To mitigate the effect of this on the anthropogenic $CO_2$ emission monitoring, we investigate the effect of the AOD threshold on the fraction of acceptable $XCO_2$ data. We find that relaxing the MODIS AOD threshold from 0.2 to 0.5, which is the goal for the CO2M, increases the fraction of acceptable data by 14 percentage points globally, and by 31 percentage points for urban areas.

## 1 Introduction

Anthropogenic emissions of carbon dioxide ($CO_2$) will be monitored operationally in this decade using atmospheric measurements to support the Global Stocktake and provide independent information for tracking national emission reductions outlined in the Paris Agreement (Janssens-Maenhout et al., 2020). While ground-based greenhouse gas measurements are mainly available in developed countries – with limited coverage and representativeness – satellite-based $XCO_2$ information will be irreplaceable in areas where ground-based measurements are not made. An essential monitoring component will be the Copernicus Anthropogenic $CO_2$ Monitoring Mission (CO2M; Meijer et al. (2023)). The key purpose of the observations is to provide means for an independent verification of nationally reported emissions and, therefore, the focus and the challenge of the CO2M will be in the need to make accurate and precise observations of anthropogenically polluted environments.

The existing satellite $XCO_2$ products from JAXA's Greenhouse Gases Observing Satellite (GOSAT; (Yokota et al., 2009)), NASA's Orbiting Carbon Observatory-2 (OCO-2; (Crisp et al., 2004)), and the Chinese TanSat (Yang et al., 2018) are focused on global $CO_2$ observations and have been developed to inform flux inversion models for quantifying the large-scale sources and sinks of $CO_2$ (e.g. Houweling et al. (2015); Crowell et al. (2019)). In assimilating satellite data to inverse model systems, the reliability of data has been preferred at the cost of not achieving full global coverage; thus, the observations of potentially deteriorated quality are filtered in the postprocessing. One of the known factors affecting $XCO_2$ retrieval accuracy and precision are atmospheric aerosols: scattering and absorption by aerosols affects the light path of radiation and complicate the interpretation of the signal (Butz et al., 2009; Guerlet et al., 2013; Connor et al., 2016; Lamminpää et al., 2019; Rusli et al., 2021). Therefore, retrievals made in aerosol-loaded conditions are mostly filtered out (e.g., (O'Dell et al., 2018)). In the advent of CO2M and other missions targeting anthropogenic signals, the focus of flux estimation is shifting from using satellite data from pristine, aerosol-free scenes to the need to also observe aerosol-contaminated, polluted atmospheres. The goal is to enable reliable quantification of local and regional anthropogenic $CO_2$ emissions, but this poses new challenges to the satellite retrievals.

In the NASA Atmospheric $CO_2$ Observations from Space (ACOS) retrieval algorithm for OCO-2 observations, the aerosol properties are retrieved as part of the full-physics retrieval, and are known to have high uncertainties, in particular for high aerosol loads (O'Dell et al., 2018). The potential to improve the co-retrieval of aerosols and $XCO_2$ has been emphasized in recent studies (Lamminpää et al., 2019; Sanghavi et al., 2020). A systematic, statistical study on the long data record of OCO-2 observations in quantified aerosol conditions can increase understanding of the potential aerosol effects on $CO_2$ retrievals and support preparations towards the CO2M observations. Reliable information of atmospheric aerosols can be obtained from ground-based instruments and from satellite-based instruments (and algorithms) specialized to detect aerosols, such as Moderate Resolution Imaging Spectro-radiometer (MODIS, Levy and Hsu (2015)). In the latter case, the favorable orbital configuration of OCO-2 and Aqua satellites as part of the Afternoon-train constellation ensures optimal coverage for collocated observations. This enables an expansion of the evaluation beyond the traditional approaches that are centered around ground-based validation sites (e.g., the Total Carbon Column Observing Network; TCCON Wunch et al. (2011)) from which only a small fraction represent an urban environment.

In this paper, we evaluate the OCO-2 level 2 product from the point of view of aerosols by comparing the OCO-2 estimated aerosol properties to the MODIS/Aqua Dark Target aerosol product. We study how well the current ACOS quality filtering works in different aerosol conditions, focusing in particular on heavy aerosol conditions and urban environments. The focus of this paper is on the statistical analysis of a global, multiyear dataset. For complementarity, we will also use all available TCCON data as a subset of the study and to estimate aerosol and $CO_2$ co-emission.

## 2 Data

### 2.1 OCO-2

NASA's Orbiting Carbon Observatory -2 (OCO-2) is an atmospheric carbon dioxide ($CO_2$) observing mission with a diffraction-grating spectrometer onboard a polar-orbiting satellite. OCO-2 makes passive observations of backscattered solar radiation in the near- and shortwave infrared wavelengths. It has a ground-pixel size of approximately 1 km x 2 km, and covers a swath width of 10 km, with a 16-day revisit time.

We use OCO-2 daily Lite files (V10r) (OCO-2 Science Team et al., 2020), produced by the OCO-2 project at the Jet Propulsion Laboratory, California Institute of Technology, and obtained from the OCO-2 data archive maintained at the NASA Goddard Earth Science Data and Information Services Center (O'Dell et al., 2018; Wunch et al., 2017; Taylor et al., 2023). The aerosol parameters of the ACOS algorithm include five scatterers, which are two cloud types (water and ice), two tropospheric aerosol types and a stratospheric aerosol type (sulfate). The two most representative types of tropospheric aerosols out of five possible types (dust, sea salt, sulfate aerosol, organic carbon, and black carbon) are drawn from collocated 3-hourly aerosol fields from Goddard Earth Observing System Model, Version 5, Forward Processing for Instrument Teams (GEOS-5 FP-IT; see Crisp et al. (2021)). From the large number of data products provided by the ACOS Level 2 full-physics (L2FP) retrieval algorithm, we use mainly the estimates of the $CO_2$ column-averaged dry-air mole fraction ($XCO_2$), the total aerosol optical depth (AOD) values, and the $XCO_2$ quality flag.

### 2.2 MODIS

We use the level-2 (L2) Moderate Resolution Imaging Spectro-radiometer (MODIS) Collection 6.1 atmospheric aerosol product from the Aqua platform (MYD04_L2) as reference aerosol data (Levy and Hsu, 2015). The MODIS Dark Target (DT) algorithm (Levy et al., 2013) is available over ocean and dark (e.g., vegetated) land surfaces, while the MODIS Deep Blue (DB) (Hsu et al., 2004) covers land areas including bright surfaces. As we are mainly interested on the effect of aerosols on $XCO_2$ over urban areas, we concentrate on MODIS retrievals over land surfaces and use mainly the 10 km MODIS DT product over land; results for DB are shown in Appendix A. While the global aerosol optical depth (AOD) patterns are somewhat different between DT and DB, we find that the global statistics and conclusion regarding the connection to $XCO_2$ retrievals are largely the same. Collocation with the higher spatial resolution MODIS 3 km aerosol product (MYD04_3K; Remer et al. (2013)) was tested for one year (2018). The results did not differ significantly from the corresponding subset when using the

10 km DT product (not shown). Due to the considerably larger computational burden of the 3 km data, the full dataset was processed only with the 10 km product. Previous studies have shown that the 3 km and 10 km products perform very similarly on the global scale (Gupta et al., 2018; He et al., 2017). For more detailed case studies the use of MODIS 3 km product could be beneficial, but that is beyond to scope of this exercise.

Both Aqua and OCO-2 are in the Afternoon-train satellite constellation following similar orbital tracks allowing fair collocation between the instruments. MODIS data used in this study were obtained from the NASA Level-1 and Atmosphere Archive & Distribution System Distributed Active Archive Center (LAADS DAAC) (https://ladsweb.modaps.eosdis.nasa.gov, last access: 14 November 2024). Five years of data from 2015 to 2019 were processed. Due to the large size of the original MODIS L2 aerosol data, the data were pre-processed before collocating with OCO-2 data to create daily files which contain a reduced number of original data fields and cloud-screened pixels only. MODIS quality flag was applied to remove the poor quality pixels (MODIS quality flag 0). We also tested using more stringent quality filtering, keeping only the best quality MODIS data (quality flag 3). Although this reduced the number of matches with OCO-2 by nearly 30% and reduced the global average AOD by 0.02, it did not affect the conclusions of our work. Note that the MODIS quality flag is systematically applied throughout the results in this paper, while the use of OCO-2 quality flag varies. In the rest of the paper, when the use of quality flag or quality filtering is discussed, this refers to the OCO-2 quality flag.

### 2.3 TCCON

For ground-based reference $XCO_2$ measurements, we employ the Total Carbon Column Observing Network (TCCON) which consists of high-resolution Fourier Transform Spectrometers that make observations of direct sunlight in the near-infrared wavelengths. TCCON provides precise and accurate retrievals of the total column $CO_2$ abundance (Wunch et al., 2011). In this study, we use data from 26 TCCON stations to quantify the AOD dependence of $XCO_2$ (Table A4).

### 2.4 AERONET

The AErosol RObotic NETwork (AERONET) is used as ground based reference data for AOD. AERONET is a network of over 600 stations (currently) using standardised methodology and equipment to measure aerosol optical, microphysical, and radiative properties (Holben et al., 1998). The AERONET sunphotometer measurements are routinely used as reference measurements for satellite aerosol retrievals due to their high accuracy (absolute error in AOD of the order 0.01-0.02, Eck et al. (1999); Sinyuk et al. (2020)). In this work we use AERONET Version 3 level 2.0 data at 500, 675 and 870 nm to evaluate the OCO-2 total AOD (Giles et al., 2019). We consider AERONET data collocated with OCO-2 glint and nadir observations for September 2014 - February 2023.

## 3 Methods

### 3.1 Collocation of MODIS and OCO-2 data

The OCO-2 and MODIS data are collocated using the OCO-2 daily (lite) files and reduced daily MODIS files. The collocation is done by selecting the nearest MODIS pixel for each OCO-2 pixel within a $0.2^\circ \times 0.2^\circ$ area and within one hour of OCO-2 overpass (to remove possible overlapping orbits of the same day at high latitudes). To further reduce the data size, the collocated dataset includes only those OCO-2 data points for which a MODIS match is found. This reduces the number of data points to about 14% of the original OCO-2 data points for the five years considered (2015-2019). Table A1 shows the number of original OCO-2 data points and the number of collocated data points with MODIS match for each year (2015-2019). Using the MODIS DT-land retrieval removes oceans and bright surfaces such as deserts and snow covered areas, and the MODIS cloud mask and quality filtering may further reduce the number of data. This reduces the coverage of the collocated dataset with respect to the original OCO-2 data especially at high latitudes. We note that although both data products are cloud screened, possible mutual cloud contaminated pixels can cause erroneous high AOD values, which may affect the obtained correlation coefficients. Fig. A1 shows the fraction of OCO-2 pixels with a MODIS match for $1^\circ \times 1^\circ$ grid cells, and the fraction of good quality pixels (OCO-2 quality flag) for the collocated data. The collocated dataset in netcdf format is available as open data (Virtanen, 2024).

### 3.2 Collocation with TCCON

OCO-2 v10 $XCO_2$ observations were collocated with TCCON using the following criteria. Spatially, all satellite observations within 1 degrees in latitude and 1.5 degrees in longitude from a given TCCON site were collected and, for each observation, a corresponding TCCON $XCO_2$ value was assigned as the mean of TCCON $XCO_2$ retrievals within $\pm60$ minutes from each OCO-2 observation. The effect of different prior profiles in OCO-2 v10 and TCCON retrieval algorithm version GGG2020 (Laughner et al., 2024) was taken into account by adjusting the OCO-2 $XCO_2$ value, following Mendonca et al. (2021). In practice, this adjustment was very small, given the similarity of the prior profiles. The different vertical sensitivity of the TCCON and OCO-2 retrievals was taken into account by adjusting the retrieved, collocated TCCON $XCO_2$ values (Mendonca et al., 2021).

### 3.3 Collocation with AERONET

Each nadir or glint mode OCO-2 observation close to an AERONET site is matched with the ground based observations using the following criteria. Spatial collocation uses distance threshold of $0.1^\circ$ around all available AERONET sites and temporal collocation averages AERONET observation within $\pm30$ minutes of the satellite overpass. The OCO-2 observations within the $0.1^\circ$ radius are included in the comparison individually (no spatial averaging). We note that the comparison statistics are typically affected by the spatial and temporal collocation parameters (see e.g. Virtanen et al. (2018)). Different sampling radii and time windows were tested with a subset of data, with minor effects on the results. With the abundance of AERONET sites, we could afford a smaller sampling area than that used for TCCON data. A simple average of AOD values at 675 and 870 nm is used to evaluate the effect of wavelength difference (see Fig. 3). While this simple approach may not be the most accurate, it is sufficiently accurate for our purposes. A more accurate method for the wavelength scaling using the Ångström exponent from AERONET was tested for a subset of data, and we did not find significant differences in the results.

### 3.4 Aggregation of collocated data

Analysing the collocated data of this size ($\sim$ 10 M points for a year) requires some aggregation before plotting. Two approaches have been applied: **1)** Data fields are aggregated to an AOD vs. AOD grid, i.e. data points falling in certain MODIS AOD bin and certain OCO-2 AOD bin are averaged (e.g. Fig. 7). For MODIS, we use AOD at 550 nm and for OCO-2 the total AOD data field. The number of data points in each AOD matrix grid cell is also recorded (e.g. Fig. 4). **2)** In the second approach the data is aggregated to a regular lat/lon grid (e.g. Fig. 1). Optionally, the OCO-2 quality flag (QF) can be applied in the aggregation, removing low quality pixels. Aggregation is done using all available collocated data over five years (2015-2019).

### 3.5 Linear trend correction for $XCO_2$

For the multiyear dataset we use a simple detrending of OCO-2 $XCO_2$ values to compensate for the steady increase of $CO_2$ levels in order to focus more on the details of $XCO_2$ variability and possible retrieval biases. A reference date is set at 1 January 2015, and a linear increase of 2.4ppm/y is assumed and corrected for in the data (ten year global average, NOAA Global Monitoring Laboratory (last access: 22 April 2024)). We call this process the linear trend correction, and when applied to the $XCO_2$ data in this work, we denote this by the abbreviation LTC. While this approach allows meaningful aggregation of $XCO_2$ data over several years, it does not take into account the (spatially varying) seasonal variation of $XCO_2$.

### 3.6 $XCO_2$ anomaly

The OCO-2 $XCO_2$ anomaly is calculated for each good quality OCO-2 pixel in the collocated dataset as the difference from a local, temporally varying median value. This median is calculated from the good quality pixels in the same OCO-2 orbit, within 500 km from the pixel considered. The idea is that the yearly increase in $CO_2$ and the seasonal variation are large spatial scale effects which are captured by the 500 km portion of an orbit. When the median value is subtracted, the remaining 'anomaly' part is assumed to contain information on local sources and sinks, while the trend and seasonal effects are removed. This is an alternative way to de-trend the data, instead of applying the simple LTC. Unlike LTC, the anomaly method also effectively de-seasonalises the data. It also allows to study the covariance of AOD values and local $XCO_2$ anomalies caused by possible $CO_2$ sources and sinks. While most of the results shown in this work have been processed with the linear trend correction, the corresponding $XCO_2$ anomaly results are also shown where appropriate to support the analysis.

## 4 Results

In this section, we explore the relationships and implications of five years of global collocated MODIS and OCO-2 data, with a particular focus on how AOD differences impact $XCO_2$ retrievals. We will first consider the differences between collocated

MODIS and OCO-2 AOD data to establish the variability in aerosol estimates across different regions (Section 4.1). This provides the foundation for understanding how regional variations in AOD influence $XCO_2$ retrievals, particularly in polluted areas.

Building on this, we examine the extent to which high-AOD cases, identified using MODIS, remain in the quality-filtered OCO-2 dataset (Section 4.2). This is particularly relevant for urban regions where aerosol and $CO_2$ emissions are correlated, making accurate detection and handling of high-AOD cases essential for reliable monitoring of anthropogenic $CO_2$ emissions. In Section 4.3, we explore the statistical relationship between AOD and $XCO_2$ using TCCON data as reference, and considering both real atmospheric co-emission effects and aerosol-induced retrieval biases. In this context, in order to remove the effect of increasing $XCO_2$ values over the five years, we apply the simple linear trend correction (LTC) described in the Methods section. As an alternative de-trending option for $XCO_2$ we use anomaly data (see Methods), which is useful in removing also the seasonal effect, preserving ideally local-scale spatial variability.

Finally, Section 4.4 examines how using different AOD thresholds for quality filtering impact data coverage, with a focus on the correlation between AOD and $CO_2$ emissions. Since high-AOD cases often correspond to high $CO_2$ emission regions, limiting retrievals to low AOD introduces a sampling bias by disproportionately removing these high-emission cases. Relaxing the AOD threshold increases coverage, particularly in urban areas, complementing the previous analyses by ensuring a more representative dataset for monitoring anthropogenic $CO_2$ emissions.

### 4.1 Spatial AOD comparison

Figure 1 a) shows MODIS DT AOD at 550 nm aggregated to a $1^\circ \times 1^\circ$ lat/lon grid for 2015-2019 for quality-filtered collocated data (the MODIS quality flag is always applied; here we use also the OCO-2 quality flag) over land. High AOD areas due to anthropogenic aerosol emissions are seen in particular in parts of Asia and elevated aerosol loads due to dust are seen over various desert areas around the globe. MODIS Dark Target observations are not available over bright surfaces such as large deserts and snow-covered areas, which explains the gaps seen on the map. Figure 1 b) shows the AOD difference between OCO-2 and MODIS. Note that the OCO-2 AOD is retrieved at 755 nm, while the MODIS AOD is obtained at 550nm; the effect of the wavelength difference will be discussed below. The largest differences in AOD appear to be concentrated largely in the high AOD areas in parts of Asia, where OCO-2 AOD is lower than MODIS AOD. Also, for several areas with low MODIS AOD, OCO-2 shows higher values (positive AOD difference), e.g. in parts of Brazil and Australia. These positive difference values are related to the MODIS DT algorithm permitting small negative AOD values (Sayer et al., 2014). In short, the negative values mean that the AOD is low, but the exact value is not certain. While the negative values are unphysical, they are kept in the data in order to avoid a positive bias in the data. The AOD difference is also positive for the Sahel region where the MODIS DT values in the collocated dataset are low. The Sahel area is known to have occasional high AOD caused by desert dust. Part of these cases are removed by the OCO-2 quality filtering. MODIS DT algorithm has lower AOD values compared to MODIS Deep Blue algorithm in this region. The AOD map and AOD difference map for MODIS DB are shown in the Fig. A2. We see that MODIS DB shows higher AOD than OCO-2 more often than MODIS DT. A limited collocation test made with MODIS 3 km aerosol product for the year 2018 shows slightly enhanced coverage but otherwise very similar AOD patterns as the 10 km DT product.

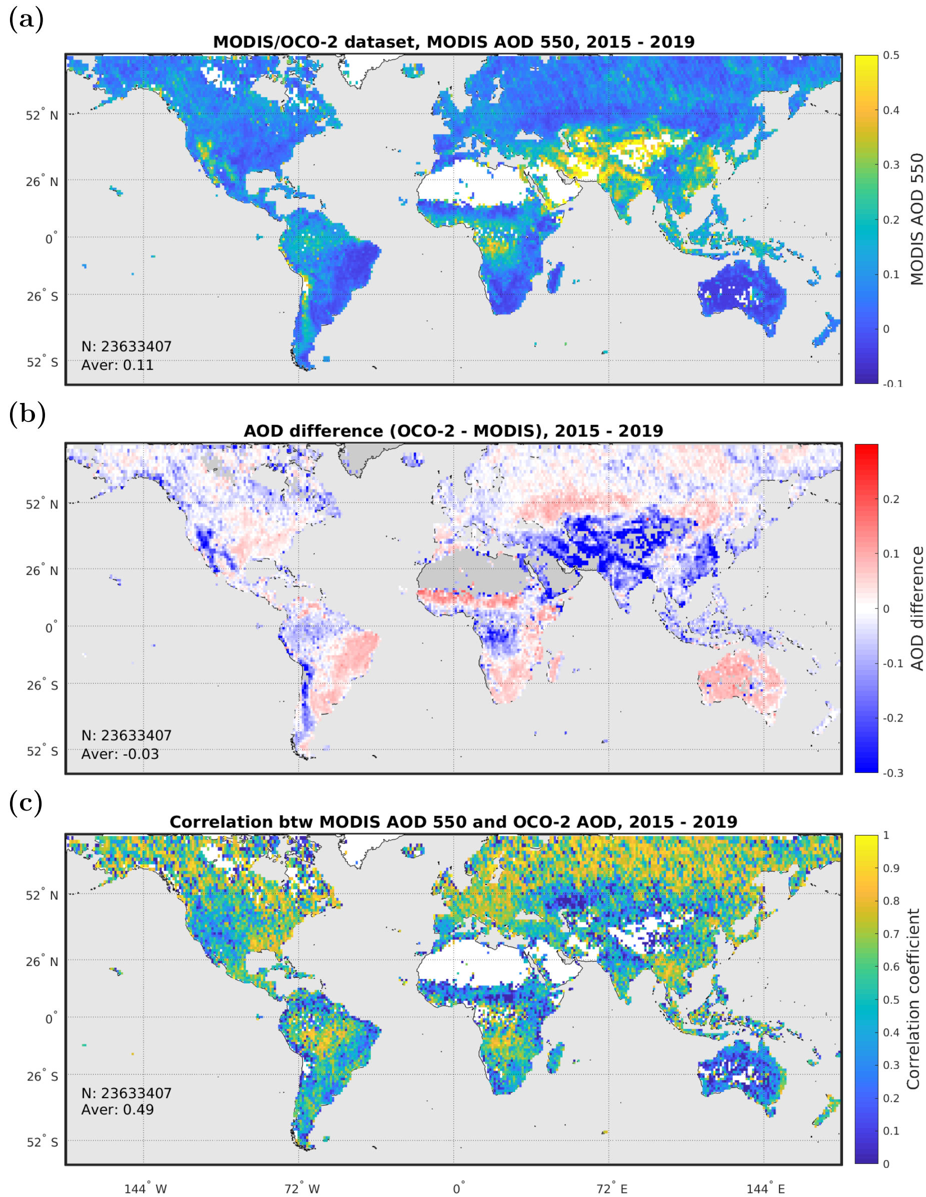


**Figure 1.** Collocated OCO-2 v10 and MODIS Aqua DT-land dataset five year $1^{\circ} \times 1^{\circ}$ aggregate maps for quality filtered data. **a)** MODIS AOD at 550 nm. **b)** AOD difference (OCO-2 - MODIS). **c)** Correlation between MODIS and OCO-2 AOD values for $1^{\circ} \times 1^{\circ}$ grid cells.

Figure 1 c) shows Pearson correlation coefficient R between MODIS AOD at 550 nm and OCO-2 total AOD for $1^\circ \times 1^\circ$ grid cells for five years. The data is rather noisy, but regions with particularly low correlation are seen, including Australia, Sahel, Western USA and the arid regions of Central Asia. These areas are characterized by bright surfaces, indicating that the surface reflectance treatment in the algorithms might explain part of the differences in AOD. We note that MODIS DB shows roughly similar patterns (Fig. A2 c), including low correlation over bright surface areas. Good correlation is observed in Europe, northern high latitudes, and over tropical rainforests. Figure 2 a) shows a global timeseries comparison for MODIS and OCO-2 AODs. The correlation coefficient calculated from monthly temporal bins (R=0.53) is similar to the average spatial correlation in Fig. 1 c) (R=0.49). We note that possible mutual cloud contamination of collocated data points could lead to erroneous high AOD values for both instruments, possibly leading to higher correlation values than without cloud contamination. However, data from each satellite is cloud screened with their respective cloud masks, and the vast majority of data is in the low AOD region, reducing the probability of large bias.

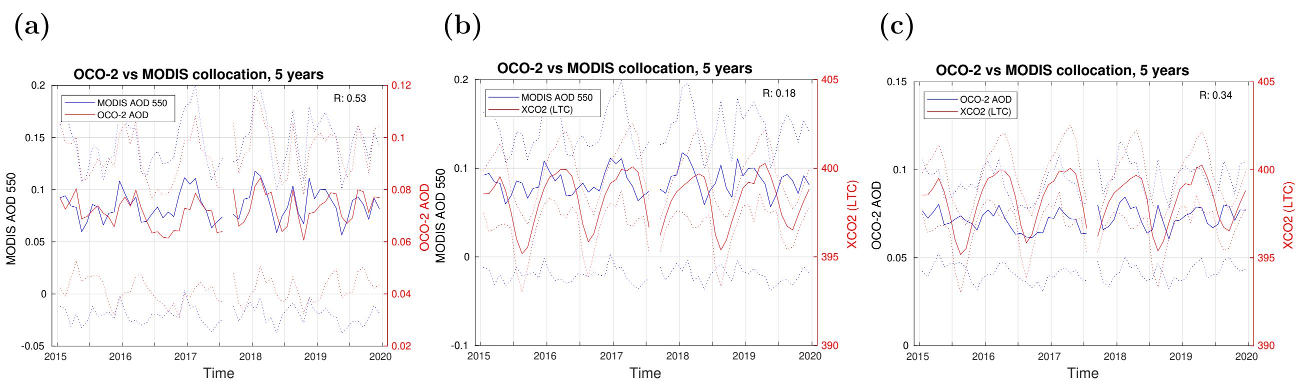


**Figure 2.** Temporal bin plots (3-week mean values) for the global, quality filtered collocated OCO-2/MODIS dataset. Dotted lines show the interquartile range. Correlation coefficients R are calculated from the temporal bin values. Comparison of **a)** MODIS and OCO-2 AOD, **b)** MODIS AOD and OCO-2 $XCO_2$, **c)** OCO-2 AOD and $XCO_2$. The positive correlation suggests that there is temporal covariance between AOD and $XCO_2$.

Here we point out that the MODIS AOD is evaluated at 550 nm wavelength, while the OCO-2 total AOD value corresponds to 755 nm, and the two are hence not directly comparable. We do not expect to see a one-to-one correspondence between the two. The sensitivity of AOD on the wavelength depends on the aerosol size distribution and other properties. In general, for typical ambient aerosols, it is expected that the AOD is smaller at 755 nm, as suggested by the data. One way to scale the AOD obtained at one wavelength to other wavelength is to use the Ångström exponent. While MODIS-based estimates of Ångström exponent exist, they are not reliable over land (Levy et al., 2010). To obtain a rough idea about how the wavelength difference might affect the AOD comparison on global scale, we have used the Ångström exponent from collocated MERRA-2 monthly climatology (Global Modeling And Assimilation Office, last access: 22 April 2024) to scale the OCO-2 AOD values to 550 nm, which can be considered as a reference wavelength used in many satellite aerosol products. The result suggests that the low bias in OCO-2 AOD compared to MODIS is only slightly reduced by the scaling (Fig. A3). A bivariate linear fit for OCO-2 AOD (at 755 nm) as function of MODIS AOD (at 550 nm) gives a slope 0.3, while a fit using OCO-2 AOD scaled to 550 nm gives a slope 0.4 (without the OCO-2 quality filtering).

The use of MERRA-2 data potentially induces high uncertainty to the spectral conversion. We use this method merely to get a rough estimate of the effect of the wavelength difference on the AOD difference. This is done only in a statistical sense for the global dataset, understanding that the high uncertainties involved with the scaling do not allow for a more detailed comparison. The main conclusion drawn from this is that while the slope of OCO-2 AOD against MODIS AOD is 0.3 before spectral scaling, it is 0.5 after the scaling, i.e. the wavelength difference explains part, but not all, of the difference. The spectral conversion was repeated with a smaller subset of data using Ångström exponent from AERONET, and the results largely agreed with the global dataset.

Comparison of OCO-2 AOD with AERONET shows similar results (Fig. 3). A linear fit of OCO-2 AOD against AERONET AOD at 500 nm gives a slope 0.3, while a fit against AERONET AOD scaled to 770 nm gives a slope 0.53. The slope is further increased when a more recent version of OCO-2 algorithm is used. The similarity of these results supports the assumption that MODIS AOD can be used as reference data in evaluating the OCO-2 performance. The MODIS aerosol products have been extensively validated, with a typical correlation coefficient R$\sim$0.9 against AERONET (Levy et al., 2013; Sayer et al., 2014; Wei et al., 2019). We do not repeat the MODIS AOD product validation against AERONET in this work, but we have compared the MODIS part of the collocated OCO-2/MODIS dataset to AERONET with similar sampling as used for OCO-2. This differs from the typical validation in that the sampling is not optimal for MODIS but limited to the pixels collocated with OCO-2. As expected, this sampling leads to slightly reduced validation metrics against AERONET (R$\sim$0.8, small bias), but the metrics are still better than for OCO-2. Hence, we are confident that although MODIS AOD product certainly has higher uncertainty than AERONET, it helps to the extend the evaluation of OCO-2 AOD to the global scale.

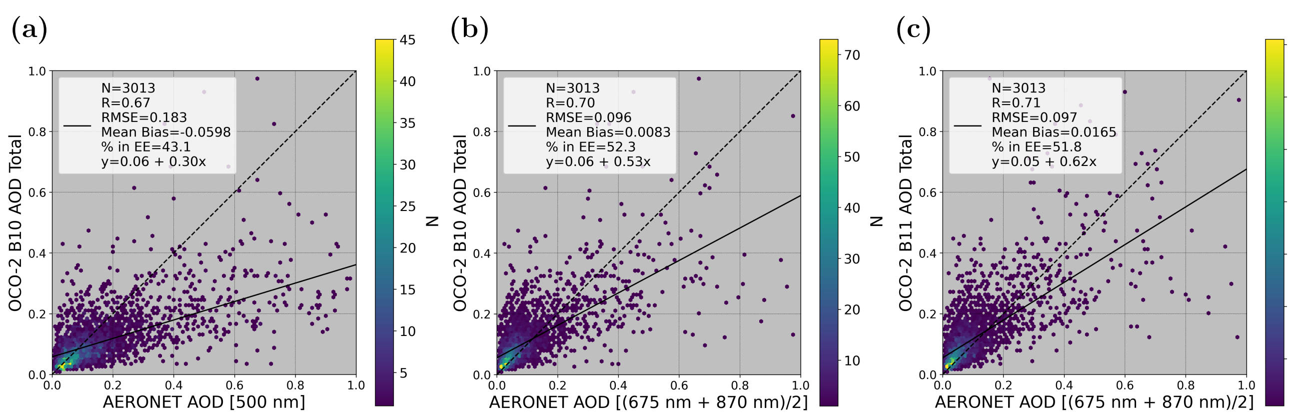


**Figure 3.** Comparison between OCO-2 and AERONET for all collocated data through February 2023. **a)** AERONET AOD at 500nm. **b)** AERONET AOD scaled to 770 nm by simple average. **c)** OCO-2 version B11.

The OCO-2 quality filtering applied to the collocated dataset heavily affects the AOD comparison shown in Figure 1. Because the cases where OCO-2 retrieves large AODs are removed by the quality filtering, the aggregated MODIS DT AOD values are much lower than they would be for unfiltered MODIS data. The quality filtering also causes a sampling bias between MODIS and OCO-2 AOD data, since not all cases with high MODIS AOD are removed. Statistics for AOD in different subsets are shown in Tables A1 to A2. The correlation is better for unfiltered data (Table A2).

Finally, we note that the OCO-2 retrieval algorithm ACOS is not an aerosol retrieval algorithm and the total AOD value included in the product is only one of more than fifty components in the full physics retrieval. Incorrect AOD values in the ACOS retrieval may be compensated by other retrieval parameters, and a difference between MODIS and OCO-2 AOD values does not necessarily indicate erroneous $XCO_2$ retrieval. Our focus here is not to evaluate the AOD component of ACOS retrieval as such, but to study the statistical relationships using MODIS AOD as independent reference data. We also note that the collocation between MODIS 10 km AOD product and the OCO-2 observations at higher spatial resolution (approximately $1{\times}2$ km$^2$) affects the comparison. The collocation approach applied here, using the closest MODIS pixel for each OCO-2 data point, is the simplest possible. The simple approach was chosen to enable processing the large dataset efficiently, and more sophisticated collocation for detailed case studies are considered elsewhere. However, we made a limited test with the MODIS 3 km aerosol product for the year 2018 to study the effect of aerosol data resolution. This increased the number of matches with OCO-2 by 38% with little effect on the results: average $XCO_2$ value of the collocated dataset increased by 0.02 ppm and the average MODIS AOD increased by 0.01 for the unfiltered dataset.

The expected error envelope for MODIS DT AOD is $\pm 0.05 + 0.15\tau_{\mathrm{A}}$ for reference (AERONET) AOD $\tau_{\mathrm{A}}$ (Levy et al., 2010, 2013), indicating a high relative uncertainty at low AOD values. However, the absolute value of AOD (or the absolute difference between MODIS and OCO-2) at the very low levels is not crucial for the accuracy of the $XCO_2$ retrieval, since the effect of aerosols is expected to be small for low AODs. In addition, the cases where OCO-2 severely overestimated AOD are not seen in the quality filtered dataset, as the cases with OCO-2 AOD over 0.2 are removed by the standard quality filtering (O'Dell et al., 2018). Hence, from the point of view of the aerosol effect on the $XCO_2$ retrievals, the most important areas are those with AOD difference below -0.2 (blue areas in Fig. 1 b), where OCO-2 AOD is significantly lower than MODIS AOD. In the following we will separate the data into different AOD difference subsets to study this in more detail.

To conclude, in this section we considered the differences between collocated the MODIS DT AOD product and the OCO-2 total AOD component. We find that the AOD difference depends on region. OCO-2 tends to overestimate the aerosol load in regions with low MODIS AOD. More important for the $XCO_2$ retrievals, OCO-2 tends to severely underestimate AOD in the high MODIS AOD regions (including areas with high anthropogenic emissions), which may have an effect on the $XCO_2$ retrievals in these regions.

### 4.2 Effect of AOD discrepancy in OCO-2 quality filtering

In this section we will compare the OCO-2 total AOD component to MODIS AOD statistically for the full collocated dataset using e.g. density scatter plots. Specifically, we address the question of how well the OCO-2 quality filtering works from the point of view of aerosols. The OCO-2 quality filter uses an AOD threshold of 0.2, among several other tests, to remove heavy aerosol conditions. We use collocated MODIS AOD data to assess the performance of the OCO-2 AOD filter.

Figure 4 shows joint histograms of five years of collocated OCO-2 and MODIS AOD data (over 40 million collocated data points). In panel a) we show all data, without OCO-2 quality filtering. In panel b) we have applied filtering using the OCO-2 quality flag (O'Dell et al., 2018), which identifies potentially bad quality retrievals affected by, e.g., clouds or high aerosol loads, and removes the results with OCO-2 AOD higher than 0.2. The dashed red line shows bin-averaged OCO-2 AOD data for MODIS AOD bins (fifty bins with width 0.02; see also Fig. A3 a) for a box plot). We see that OCO-2 AOD is systematically low with respect to MODIS AOD (mean MODIS AOD is 0.15, mean OCO-2 AOD is 0.12), except for the lowest MODIS AOD values where OCO-2 has higher AOD. The overestimation at the low AOD end may be related to the water and ice aerosol components included in the OCO-2 total AOD. These two AOD components are included in the ACOS retrieval to account for possible residual cloud contamination, while the MODIS aerosol retrieval does not have corresponding elements. Preliminary study shows elevated water and ice AOD values at low MODIS AOD values, but a more detailed study, beyond the scope of this work, would be required to confirm this. The dashed green line shows a bivariate linear fit, which follows closely the binned mean values with a slope 0.33 for the unfiltered data. Naturally, the quality filtering affects the binned averages at the high MODIS AOD end, where a larger fraction of the data with high OCO-2 AOD are removed. This causes deviation of the binned averages from the linear behaviour and is reflected on the lower slope (0.18) for the linear fit.

The Pearson correlation coefficient for the unfiltered data is 0.60, reducing to 0.52 for the data filtered with the OCO-2 quality filter. The large spread of the data reflects the fact that the ACOS algorithm is not optimized for AOD retrieval, as discussed above. Considering this, the obtained correlation with MODIS AOD can be considered acceptable. Note that in the collocated dataset the MODIS data is often the limiting factor (Table A1), already removing data over bright surfaces and in proximity of clouds. Applying the OCO-2 quality filter further reduces the collocated data to 56% of the original collocated data points. We note that only 15% of the original data is removed by the total AOD threshold of 0.2, while 29% are removed by other quality tests. The lower correlation coefficient of the quality filtered dataset reflects the imbalance between OCO-2 and MODIS in the AOD distribution of data points removed by the OCO-2 quality filter.

The dotted black lines in Fig. 4 at AOD threshold of 0.2 divide the AOD matrix into four quarters Q1-Q4. The threshold 0.2 corresponds to the current limit for good quality retrievals in OCO-2 over land. We note that since the wavelength-corrected linear relation between the two instrument is roughly $\mathrm{AOD_{MODIS}} \sim 2.5\ \mathrm{AOD_{OCO-2}}$, a more appropriate AOD threshold for MODIS could be 0.5. For simplicity we use here the same limit 0.2 for both instruments, but in section 4.4 we study the effect of filtering the data with AOD threshold 0.5 applied to MODIS data. The first quarter Q1 with AOD from both instruments below 0.2 contains most of the data (68.5%). The second quarter Q2 contains data with $\tau_{\mathrm{OCO-2}} \leq 0.2$ and $\tau_{\mathrm{MODIS}} > 0.2$ (16.5%). These data points are assumed to have low AOD in the OCO-2 retrievals, but according to MODIS there can be quite heavy aerosol loads, which might affect the $XCO_2$ retrievals. Q3 contains data points with AOD above 0.2 for both instruments (10.8%).These data points are removed when the OCO-2 quality filtering is applied, which is appropriate considering that heavy aerosol conditions should be avoided in $XCO_2$ retrievals. The last quarter Q4 includes data points for which $\tau_{\mathrm{OCO-2}} > 0.2$ and

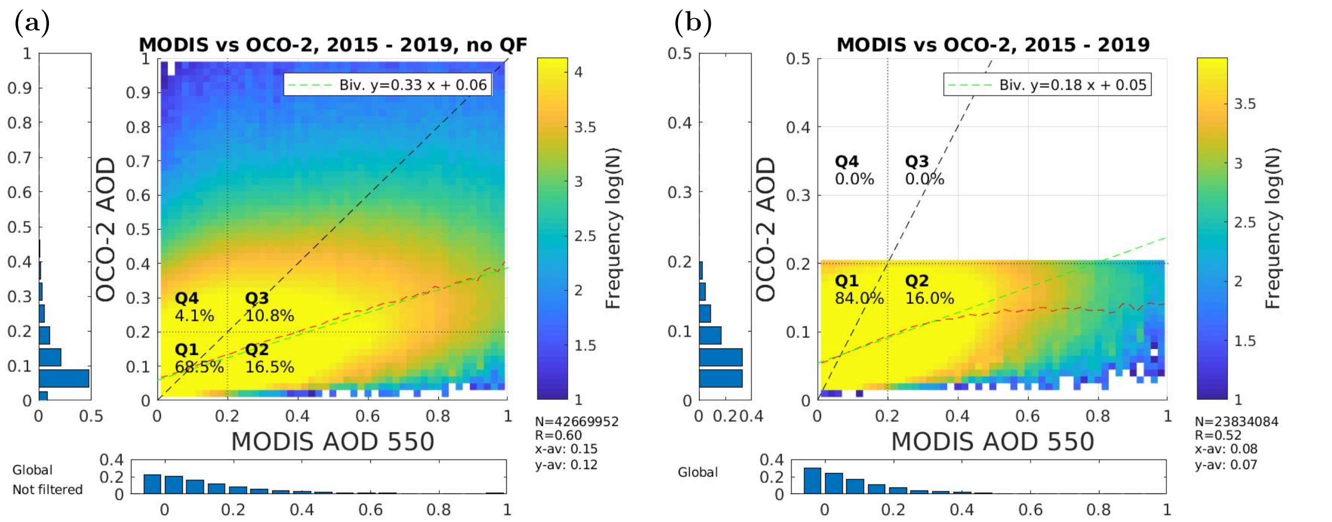


**Figure 4.** Number of collocated data (logarithmic color scale) for each 'AOD grid cell' ($50 \times 50$ cells of AOD width 0.02). Left: all data, right: good quality data only. The dashed red line shows average OCO-2 AOD for each MODIS AOD bin. The dashed green lines shows a bivariate linear fit. The dotted black lines divide the data to four 'AOD-quarters' Q1-Q4 (see text). The text insets show the fraction of data in each quarter. The dashed black line shows the 1:1 line. The normalized AOD histograms show the distribution of data respectively for OCO-2 (left) and MODIS (bottom). The lower right text inset shows the number of data, correlation coefficient (R) and average AOD values for MODIS (x-av) and OCO-2 (y-av), respectively.

$\tau_{\mathrm{MODIS}} \leq 0.2$ (4.1%). These data are removed by quality filtering, but based on low MODIS AOD values Q4 could contain good quality retrievals.

Table 1 shows the fraction of data in different quarters of the AOD matrix and the total number of data points in the collocated MODIS/OCO-2 dataset and two subsets. The numbers are shown respectively for quality filtered (good quality) and for the unfiltered (all data) cases. The global dataset includes all available OCO-2 data from 2015-2019 which have a matching MODIS aerosol retrieval (14% of all OCO-2 datapoints, over 40 million datapoints in total, see Table A1). The urban dataset is limited to areas of dense human habitation using the urban area mask from naturalearthdata.com (Ver. 4.1.0) (NaturalEarth, last access: 22 April 2024; Schneider et al., 2009), illustrated by Fig. A5; these resulst are discussed in more detail in Section 4.3. The OCO-2/TCCON dataset contains collocated MODIS/OCO-2/TCCON data for the 26 TCCON sites listed in Table A4. The fraction of data in Q2 is considerably higher for the urban subset, reflecting the higher AOD differences between the two instruments over urban areas. We see that the quality filtering using OCO-2 quality flag removes also part of data from Q1 and Q2. The $\sim$24 million good quality data points for the global dataset compose about 56% of the total collocated data, which is about 66% of data originally in the two lower quarters Q1 and Q2.

As already noted, the MODIS DT aerosol product contains a considerable fraction ($\sim$20%) of negative AOD values. While these are obviously unphysical, they are kept in the analyses in order to not disturb the AOD distribution (Sayer et al., 2014).

| | All data | | | | | Good quality | | | | | |
|---|---|---|---|---|---|---|---|---|---|---|---|
| | Fraction of data (%) | | | | $N_{\mathrm{all}}$ | Fraction of data (%) | | | | $N_{\mathrm{QF}}$ | $N_{\mathrm{QF}}/N_{\mathrm{all}}$ |
| $XCO_2$ dataset: | Q1 | Q2 | Q3 | Q4 | ($\times 10^6$) | Q1 | Q2 | Q3 | Q4 | ($\times 10^6$) | (%) |
| Global | 68.5 | 16.5 | 10.8 | 4.1 | 42.7 | 84.0 | 16.0 | 0.0 | 0.0 | 23.8 | 55.9 |
| Urban | 52.9 | 34.2 | 11.5 | 1.5 | 0.9 | 63.8 | 36.2 | 0.0 | 0.0 | 0.5 | 61.1 |
| TCCON | 77.0 | 17.9 | 3.2 | 1.9 | 1.0 | 83.5 | 16.5 | 0.0 | 0.0 | 0.7 | 65.9 |

**Table 1.** Fraction of data in different AOD quarters for different subsets of the collocated MODIS/OCO-2 datasets. 'Global' set includes all collocated data, 'urban' subset is limited to urban areas (see text), and 'TCCON' subset is further collocated with TCCON stations.

These data are not shown in Fig. 4, but in the statistics we include the negative MODIS AOD data points to the AOD quarters Q1 and Q4, depending on the corresponding OCO-2 AOD value.

Figure 5 shows maps of the fraction of data in the two AOD matrix quarters Q1 and Q2 for the good quality data per $1^\circ \times 1^\circ$ grid cell. The map for Q1 fraction reveals that for the vast majority of land regions, average AOD is less than 0.2 for both instruments; however, large areas in South East Asia and Central Africa have a low fraction of data in the low AOD quarter, and correspondingly a higher fraction of data in Q2. Therefore, these areas are more sensitive to effects caused by high aerosol loads in the $XCO_2$ retrieval. Fig. A5 shows the fraction of data in Q1 for the urban subset.

To conclude this section, we have found that the quality filtered OCO-2 data contains a large fraction of data with high MODIS AOD, potentially affecting the $XCO_2$ retrieval quality. These data are more frequent in densely populated areas with high aerosol and $CO_2$ emissions. Hence, for monitoring anthropogenic $CO_2$ emissions with satellites, it is crucial that the high AOD cases are carefully detected and treated in the satellite retrievals.

### 4.3 Connection between $XCO_2$ and AOD

In this section we consider the possible aerosol effects in the OCO-2 $XCO_2$ retrieval. Figure 6 a) shows aggregated OCO-2 $XCO_2$ values over the globe for the collocated dataset. Visual comparison with the AOD map in Fig. 1 shows some spatial correlation between high AOD and high $XCO_2$ values. This spatial correlation between high $XCO_2$ and high AOD values may affect the $XCO_2$ statistics in two ways: First, a larger fraction of data is removed by the OCO-2 quality filtering over the high $XCO_2$ load areas. Second, considering Fig. 5 for the quality filtered data shows that areas with a large fraction of data in AOD quarter Q2 typically have high $XCO_2$ values. These heavy aerosol conditions suggested by MODIS data, which remain in the quality filtered OCO-2 dataset, may affect the $XCO_2$ retrieval quality. Figure 6 b) shows the correlation between MODIS AOD and OCO-2 $XCO_2$ for $1^\circ \times 1^\circ$ grid cells. We see particularly high correlation values for the Sahel region, parts of South-East Asia, and Western USA.

The sampling of the data (e.g. seasonal variation) affects the observed spatial features. The spatio-temporal sampling of the collocated dataset is not even, but is affected e.g. by solar zenith angle, cloudiness, and snow cover. In particular, the Northern Hemisphere high latitude areas have a relatively strong seasonal cycle of $XCO_2$ (Lindqvist et al., 2015), which is not fully captured in this aggregated dataset, as the winter months are scarcely sampled. Figure 2 b) and c) show global time series

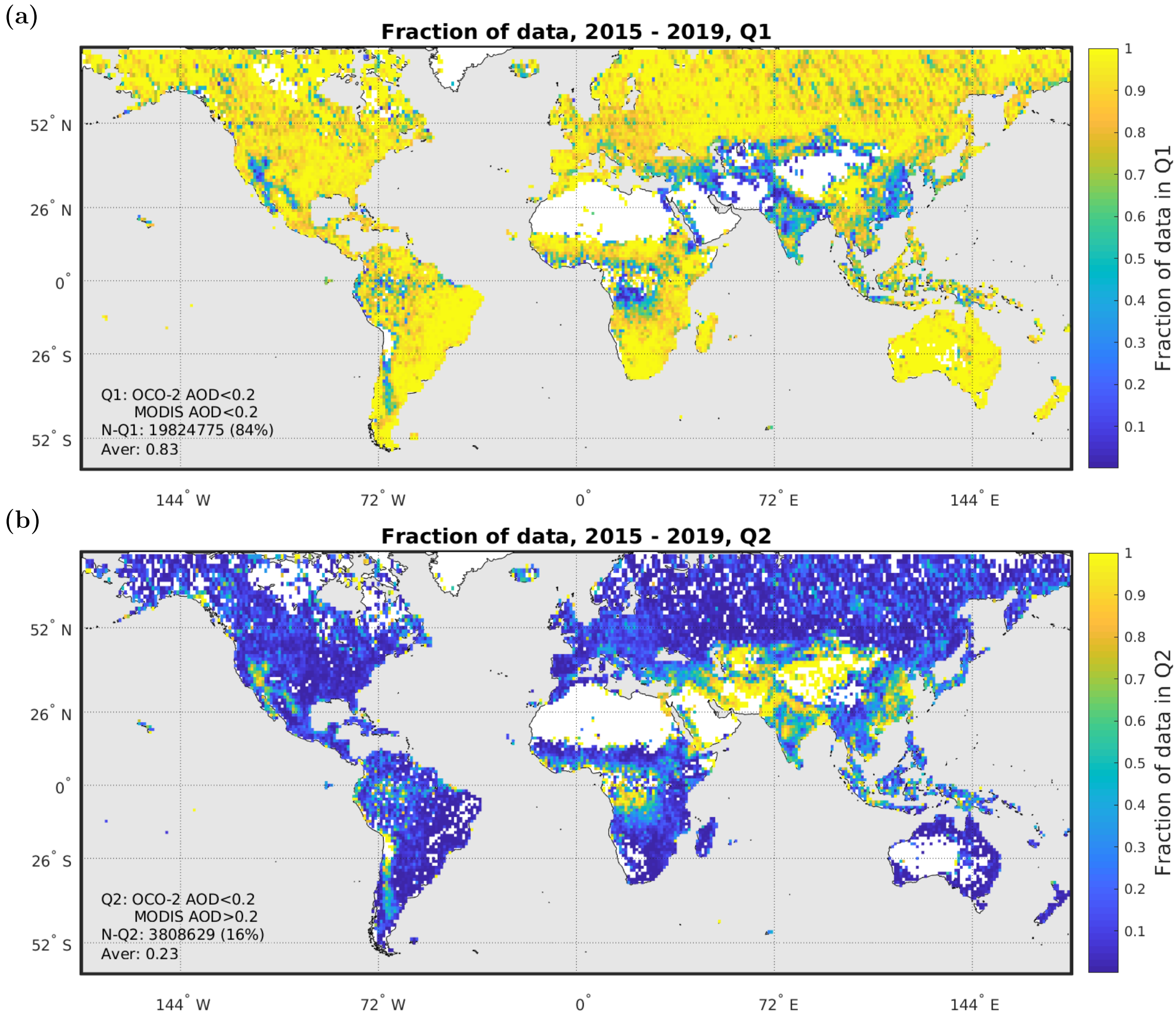


**Figure 5.** Fraction of data in AOD quarters Q1 (both AODs$<0.2$) and Q2 (OCO-2 AOD below 0.2, MODIS AOD above 0.2) for five years of data.

of collocated OCO-2/MODIS data, revealing a moderate (R=0.18) temporal correlation between MODIS AOD and OCO-2 $XCO_2$. We also emphasize that the OCO-2 swath is very narrow, and repeats over the same areas leaving relatively large gaps without data. The crude map presentation with $1^\circ \times 1^\circ$ lat/lon grid in Fig. 6 artificially fills the gaps and smooths the data, while the patchy structure of the data is still seen in the Northern high-latitude areas. Therefore, these maps serve only as rough reference indicating spatial variance in retrieved $XCO_2$ values, and one should not draw far-reaching conclusions from it. More detailed analyses are made based on the statistics from the spatio-temporally collocated subsets of the full dataset in the following.

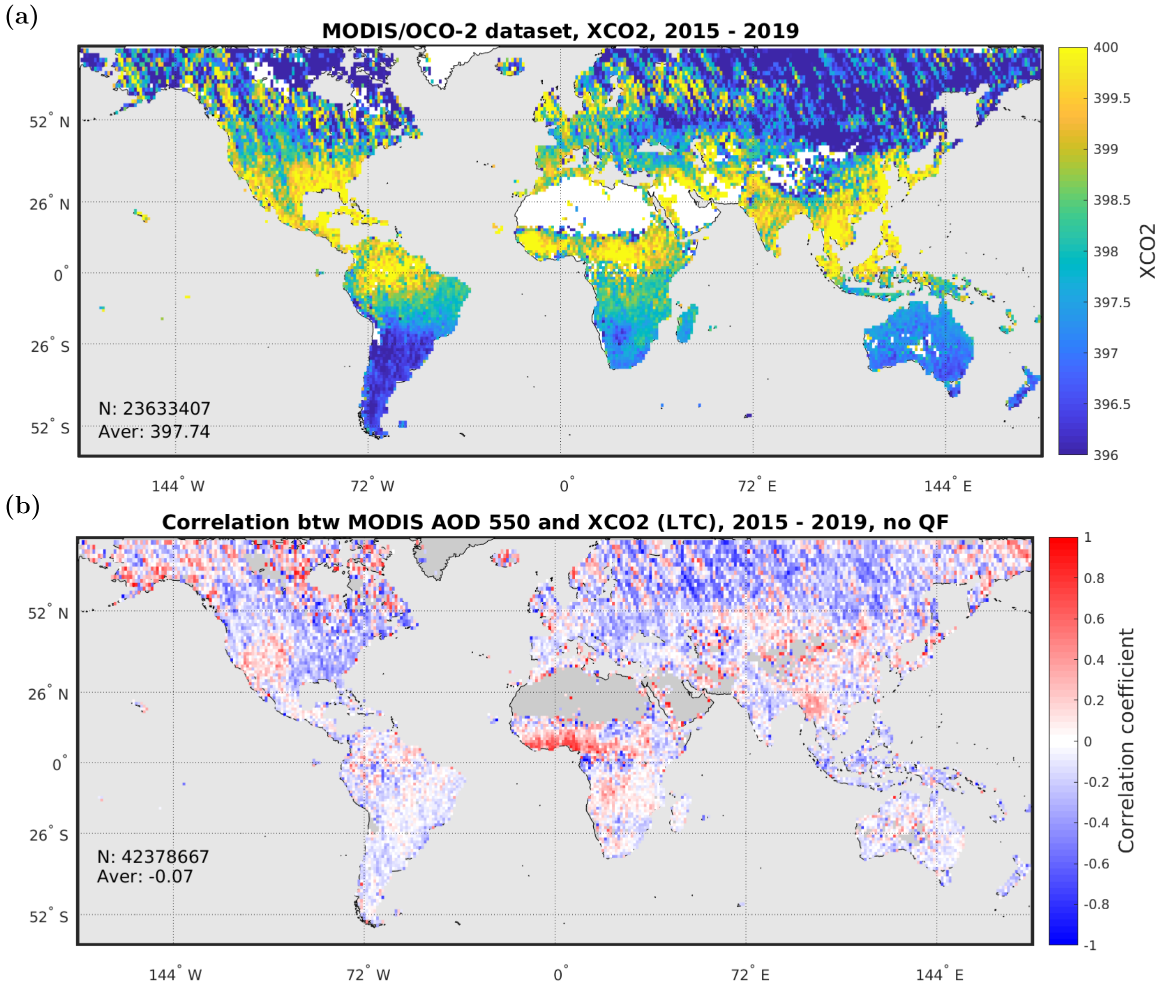


**Figure 6.** Linear-trend-corrected OCO-2 $XCO_2$ data from the collocated OCO-2 and MODIS dataset for five years (2015-2019). **a)** Quality filtered $XCO_2$ (LTC) data aggregated to $1^\circ \times 1^\circ$ grid cells. **b)** Correlation between MODIS AOD and OCO-2 $XCO_2$ for $1^\circ \times 1^\circ$ grid cells (quality filter not applied).

Figure 7 shows the retrieved $XCO_2$ values aggregated to the AOD matrix (see Fig. 4 for the number of data). When aggregating five years of data we first apply a simple linear trend correction in an attempt to remove the effect of increasing $CO_2$ values, as described in the Methods section. Figure 7 a) shows clearly, when considering all data points (no quality filtering), that the retrieved $XCO_2$ values are correlated with the relative AOD values. In AOD quarter Q4, where OCO-2 AOD is biased high compared to MODIS, we get lower $XCO_2$ values (1.3 ppm lower than the total average). In Q2, where OCO-2 AOD is biased low compared to MODIS, we get higher $XCO_2$ values (0.4 ppm higher than the total average). When quality filtering is applied (Fig. 7 b) the total average is increased by 0.2 ppm, and the Q2 average is 0.5 ppm above the total average. Table

2 shows average $XCO_2$ values for quarters Q1 and Q2 for the quality filtered data. Table A2 summarises the average $XCO_2$ values in different AOD quarters for the unfiltered data.

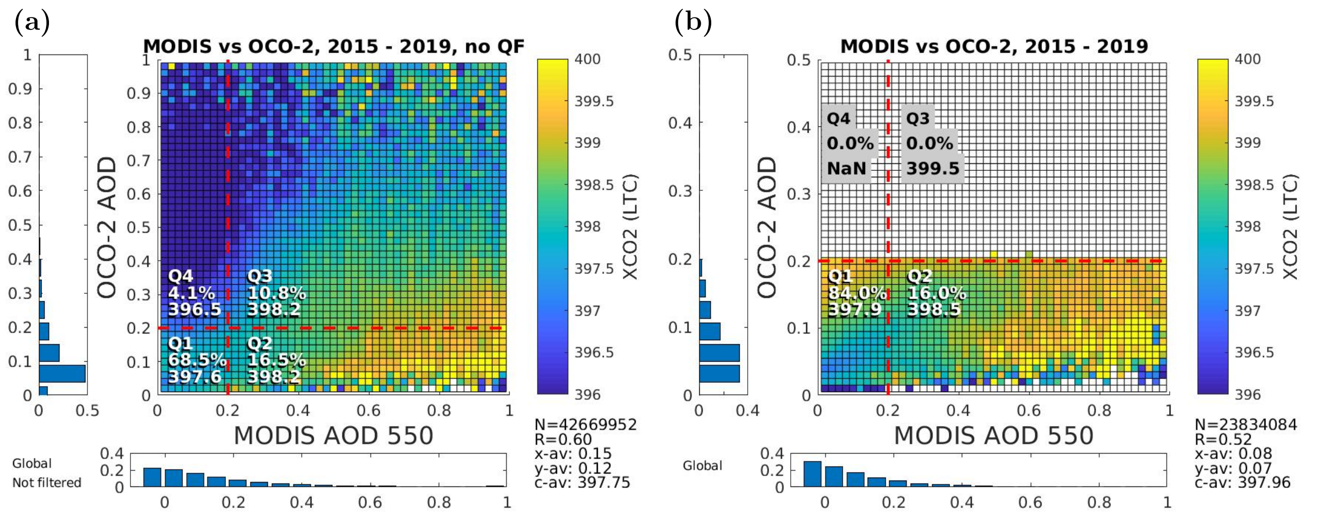


**Figure 7.** OCO-2 $XCO_2$ retrievals for five years aggregated to the AOD matrix. Linear trend correction (LTC) has been applied to the $XCO_2$ values. **a)** All data, **b)** only good quality data. The text insets on the scatter plot show the fraction of data in each AOD quarter and the mean $XCO_2$ value. The lower right hand text inset shows the number of data (N), correlation coefficient (R), average AOD values for MODIS (x-av) and OCO-2 (y-av), and average $XCO_2$ (c-av). The normalized histograms show the distribution of AOD data along each axes respectively.

| **Dataset** | **$XCO_2$ (LTC)** | | | **$\Delta XCO_2$** | | | **$XCO_2$ anom.** | | | **AOD** | | |
|---|---|---|---|---|---|---|---|---|---|---|---|---|
| (Quality filtered) | Q1 | Q2 | Total | Q1 | Q2 | Total | Q1 | Q2 | Total | MODIS | OCO-2 | R |
| Global | 397.9 | 398.5 | 398.0 | -0.14 | 0.48 | -0.04 | -0.03 | 0.05 | -0.01 | 0.08 | 0.07 | 0.52 |
| Urban | 399.1 | 399.7 | 399.3 | 1.11 | 1.72 | 1.33 | 0.00 | 0.11 | 0.04 | 0.18 | 0.07 | 0.52 |
| TCCON(1) | 399.4 | 399.9 | 399.5 | 1.37 | 1.88 | 1.46 | -0.01 | 0.12 | 0.01 | 0.09 | 0.06 | 0.45 |
| TCCON(2) | 399.1 | 399.9 | 399.2 | 1.10 | 1.86 | 1.22 | | | | 0.09 | 0.06 | 0.45 |

**Table 2.** $XCO_2$ statistics for different good quality datasets for the two AOD quarters Q1 and Q2 (see text). $\Delta XCO_2$ is calculated with respect to the reference value 398.1 ppm (the total global average value). Three datesets are used: global, urban and one collocated with TCCON. For the collocated TCCON data two $XCO_2$ values are given, from OCO-2 (labeled TCCON(1)) and from TCCON (labeled TCCON(2)), respectively. The $XCO_2$ anomaly is calculated with respect to the OCO-2 median value within 500 km. MODIS AOD is calculated at 550 nm, OCO-2 total AOD at 755 nm; R is the correlation coefficient.

As a first guess, the striking connection between $XCO_2$ and the relative AOD values between the two instruments in Fig. 7 a) could potentially be explained by the light path length used in the ACOS full physics retrieval. The top of atmosphere radiance measured by OCO-2 contains information on the total amount of $CO_2$ along the light path, and inversion of this information to $XCO_2$ values requires knowledge of the light path length, which is affected by aerosols. If the aerosol load is overestimated in the retrieval (Q4), the light path is also overestimated, and the measured $CO_2$ absorption is divided into too long distance, leading to underestimation of $XCO_2$. Similarly, if AOD is underestimated (Q2), the light path is also underestimated, causing overestimation of $XCO_2$. While the potentially bad-quality $XCO_2$ retrievals in Q3 and Q4 are removed by the quality filtering, the possible aerosol effects in Q2 remain in the quality filtered OCO-2 data. However, for Q2 the interpretation turns out to be more complicated, when the reference $XCO_2$ data from TCCON is considered, as discussed below.

The correlation between $XCO_2$ and AOD can be a sign of a retrieval bias caused by aerosols, or it can be caused by real correlation between aerosols and $CO_2$ emissions. It is entirely plausible that there is a natural correlation between AOD and $XCO_2$, stemming partially from anthropogenic (or, in case of fires or volcanoes, natural) coemission of $CO_2$ and aerosols. However, the striking feature in Fig. 7 is the dependence of $XCO_2$ on the relative AOD values between the two instruments. This dependence of $XCO_2$ on the AOD difference implies that possible biases in the aerosol treatment have an effect on the $XCO_2$ retrievals. In the following we will study these two possible causes of the observed correlation between $XCO_2$ and MODIS AOD in more detail. On one hand, to investigate the natural correlation, we will focus more on urban areas, where anthropogenic emissions are presumably more pronounced. On the other hand, we will consider the reference $XCO_2$ from 26 TCCON sites collocated with both OCO-2 and MODIS.

We have created an urban subset of the collocated data using a MODIS-based urban areas mask (NaturalEarth, last access: 22 April 2024). Figure A5 shows the urban areas (and fraction of data in Q1 for these areas). The data is reduced to slightly below one million data points (2% of all data), with mean $XCO_2$ value 1.3 ppm higher than for the global data for the quality filtered case. Similarly to the global case, lower $XCO_2$ values in Q4 and higher values in Q2 are seen for the unfiltered data (Table A2). For the urban areas there is much higher fraction of high MODIS AOD data (Q2+Q3) than globally: 36.2% (45.7%) compared to 16.0% (27.3%) for filtered (unfiltered) data (Table 1). Average MODIS AOD for urban areas is 0.18 (0.24), while for the global dataset it is 0.08 (0.15). Interestingly, for OCO-2 the corresponding values are 0.07 (0.11) and 0.07 (0.12), respectively and the high OCO-2 AOD fraction (Q3+Q4) is about the same for urban and global datasets (Table 2 and Table A2). It should be noted that earlier versions of MODIS DT aerosol retrieval had some issues over urban areas (Gupta et al., 2016), and more detailed studies on the reliability of the reference AOD values in urban areas might be useful.

Finally, there is a column for $XCO_2$ anomaly in Table 2. The OCO-2 $XCO_2$ anomaly is calculated for each good quality OCO-2 pixel in the collocated dataset as the difference from the median $XCO_2$ value calculated within 500 km for the corresponding OCO-2 orbit. This is an alternative way to de-seasonalize and de-trend the data, instead of applying the simple LTC. The idea is to study covariance of AOD values and local $XCO_2$ anomalies caused by possible $CO_2$ sources and sinks. We see that the average $XCO_2$ anomaly is negative (-0.03 ppm) in Q1 for the global dataset, indicating that average $XCO_2$ is lower in low AOD areas. Also, the anomaly is higher in Q2 further supporting the idea that local $XCO_2$ positive anomaly (source) is connected with higher AOD. For the urban areas the positive anomaly in Q2 is enhanced (0.11 ppm).

In order to further investigate to what extent the observed relation between AOD and $XCO_2$ are related to possible retrieval issues on the one hand and to the natural covariance of AOD and $XCO_2$ on the other hand, we have collocated the five year OCO-2/MODIS dataset with the ground-based data from 26 TCCON sites (see Table A4). From Table 2 we see that the TCCON

$XCO_2$ is 0.8 ppm higher in Q2 than in Q1, suggesting that there is a real positive correlation between AOD and $XCO_2$. For the OCO-2 $XCO_2$ values in the collocated TCCON dataset the difference between Q1 and Q2 is 0.5 ppm for the quality filtered data. The $XCO_2$ values are systematically higher in Q2 than in Q1 for all subsets, suggesting a positive correlation between MODIS AOD and OCO-2 $XCO_2$. In particular, the difference between Q2 and Q1 is highest for the TCCON $XCO_2$ data, which suggests that there is actually a stronger correlation between MODIS AOD and $XCO_2$ than suggested by the OCO-2 data.

Figure 8 shows joint histograms of $XCO_2$ and MODIS AOD with bivariate linear fits. In addition to the global dataset, the urban and TCCON subsets are shown. There is a small but statistically significant correlation between $XCO_2$ and AOD, and this correlation is strongest when using the TCCON $XCO_2$ data. The linear fit also shows higher positive slope for TCCON. This suggests that there is a real correlation between AOD and $XCO_2$, and this correlation is partly masked by aerosol effects in the OCO-2 retrievals. Figure 9 shows combined bin-averaged plots and linear fits for the different subsets, also as function of OCO-2 AOD and AOD difference. The linear fit slopes and correlation coefficients are summarized in Table A3. For OCO-2 AOD the slopes are also positive (and steeper). Disentangling the the effects of AOD difference between MODIS and OCO-2 and the dependence of $XCO_2$ and AOD makes interpretation of Fig. 9 c) complicated, but it is shown for completeness.

We have extended this analysis to smaller spatial and temporal subsets of data, studying, respectively, seven geographic areas: SE Asia, N Asia, N America, S America, Europe, and Australia (Fig. A7). SE Asia and Africa show a positive correlation between $XCO_2$ and AOD, while Europe and, in particular, Northern Asia have a negative correlation (not shown). Using temporal subsets, we find a positive correlation between $XCO_2$ and AOD for each year in 2015-2019, respectively, with little interannual variability. A positive correlation is also found for all seasons. Some seasonal variability is observed, with the highest slope of $XCO_2$ vs AOD in MAM.

Figure 10 shows plots similar to Fig. 8, using also OCO-2 AOD and the AOD difference on the x-axis and the $XCO_2$ difference between OCO-2 and TCCON on the y-axis, and reveals negative correlation coefficients and negative slope for the linear fits. Figure 10 a) shows a weak but statistically significant correlation between MODIS AOD and the OCO-2 $XCO_2$ bias with respect to TCCON. OCO-2 slightly overestimates $XCO_2$ for low AOD values, and underestimates at high AOD values. As with Fig. 9 c), the interpolation of Fig. 10 c) is complicated, since there are two aerosol related dependencies affecting the data. First, the AOD difference between OCO-2 and MODIS depends on the MODIS AOD in a nontrivial way as shown in Fig. 4, with OCO-2 low bias at one end and high bias at the other. Second, the $XCO_2$ bias depends also on MODIS AOD.

A post-process correction, based on systematic comparisons with the TCCON data, is routinely applied to OCO-2 $XCO_2$ data (O'Dell et al., 2018). Even when using the bias-corrected data, our comparison with TCCON reveals a residual bias which depends on the MODIS AOD. These observations further support the suggested correlation between AOD and $XCO_2$, which is partly masked by aerosols effects in the satellite retrievals. Table 3 summarizes the observed correlation coefficients and linear fit slopes for $XCO_2$ as function of AOD for the different datasets.

Disentangling the effects of AOD and $XCO_2$ differences in the comparison is not straightforward. One should also note that the TCCON sampling may affect the results. For example, not all of the included TCCON sites have data for the whole five-year period. In particular, some sites with higher AOD and $XCO_2$ values are included only towards the end of the time period. We also see that the TCCON sites are not representative for the globe in the sense that the average value of OCO-2 $XCO_2$ for

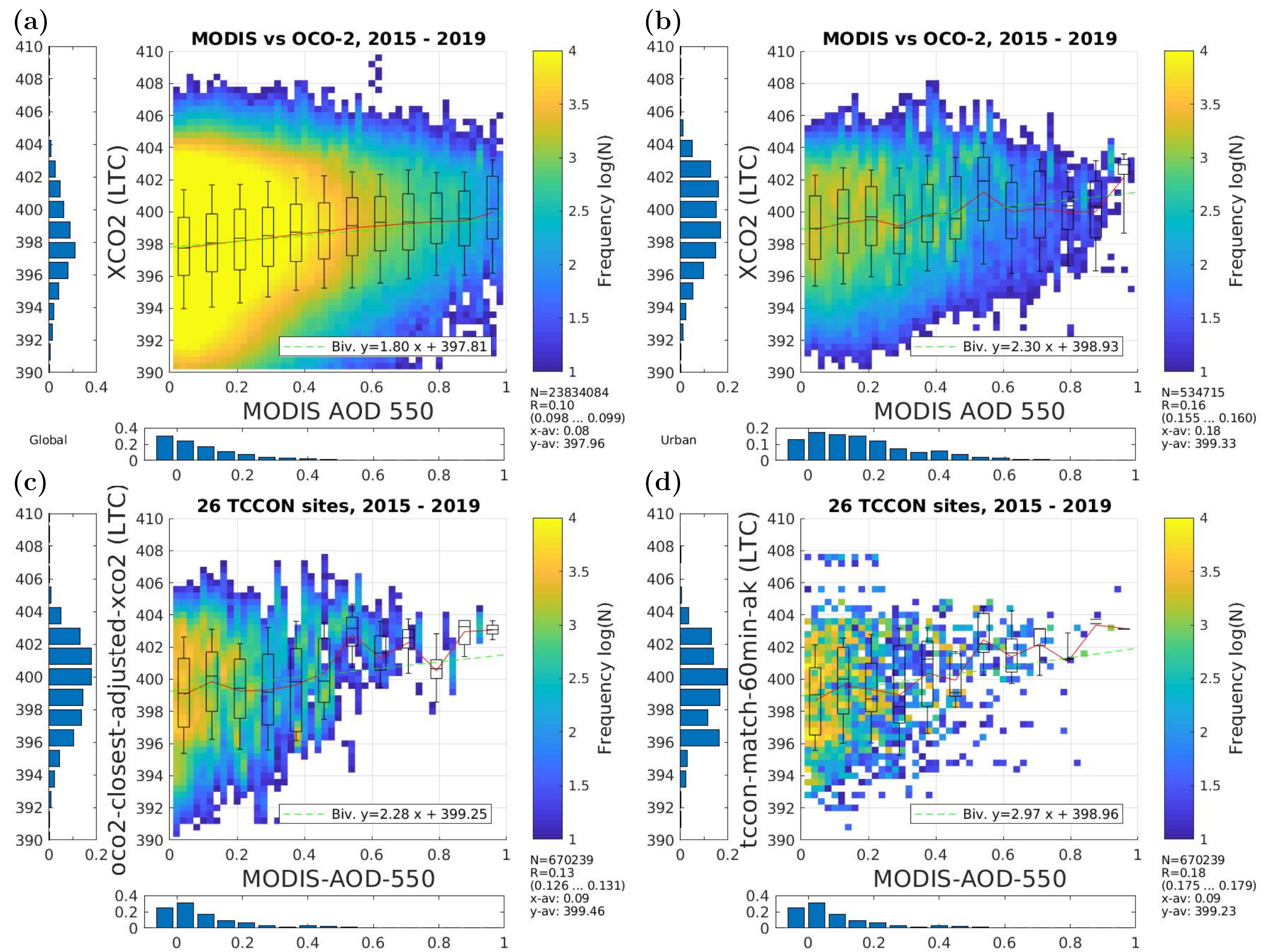


**Figure 8.** Dependence of $XCO_2$ (LTC) on MODIS AOD for different subsets (quality filtered data). The dashed red line shows binned mean $XCO_2$ values for MODIS AOD bins. The dashed green line shows corresponding bivariate linear fit. The box plot shows the interquartile range for an AOD bin, while the whiskers show 9th and 91st percentiles. The text inset on lower right corner shows similar information as in Fig. 4, with the addition of 95% confidence range for the correlation coefficient R in parentheses. **a)** Global collocated dataset. **b)** Urban data subset. **c)** Collocated MODIS/OCO-2/TCCON dataset, showing OCO-2 $XCO_2$ values (with TCCON priori adjustment). **d)** Collocated MODIS/OCO-2/TCCON dataset, showing TCCON $XCO_2$ values (60 minute average centred at the OCO-2 overpass time).

the TCCON subset is 1.5 ppm higher than the global average for data collected with MODIS (Table 2). Most of the TCCON sites are located in the northern hemisphere, with large gaps between the sites. A more detailed analysis considering individual TCCON sites respectively would be required to confirm the observed dependencies, and this is a subject of a separate study.

| $XCO_2$ (LTC) | MODIS AOD 550 | | OCO-2 AOD | | AOD difference | |
|---|---|---|---|---|---|---|
| **Dataset** | R | Slope | R | Slope | R | Slope |
| Global | 0.10 | 1.80 | 0.16 | 10.46 | -0.06 | -1.24 |
| Urban | 0.16 | 2.30 | 0.04 | 2.38 | -0.17 | -2.66 |
| TCCON(1) | 0.12 | 2.15 | 0.18 | 15.33 | -0.09 | -1.72 |
| TCCON(2) | 0.17 | 2.86 | 0.25 | 19.89 | -0.13 | -2.32 |

**Table 3.** Correlation and bivariate linear regression slopes for $XCO_2$ vs AOD for different subsets, and for AOD from different instruments (p-values $< 10^{-6}$ for all cases). For the collocated TCCON dataset, $XCO_2$ values from OCO-2 (1) and TCCON (2) are used, respectively.

To conclude this section, we find that there is a relationship between OCO-2 $XCO_2$ and MODIS AOD (Fig. 8 a). We also find a linear relation between the OCO-2 $XCO_2$ bias and MODIS AOD (Fig. 10 a). In addition, we find a relation between the AOD difference between OCO-2 and MODIS and the OCO-2 $XCO_2$ values, as shown in Fig. 7 a). Aerosols are related to OCO-2 $XCO_2$ retrievals in two ways: there is a real correlation between $XCO_2$ and AOD, due to co-emission of aerosols and $CO_2$. There is also an aerosol related bias in the OCO-2 retrievals, which acts in opposite direction than the co-emission but with smaller magnitude, thus partly masking the co-emission effect. However, we are unable to directly relate the AOD difference observed between OCO-2 and MODIS to the $XCO_2$ difference observed between OCO-2 and TCCON for the quality filtered data. This is due to the non-trivial AOD difference observed between OCO-2 and MODIS, further complicating the entanglement caused by the two competing aerosol effects.

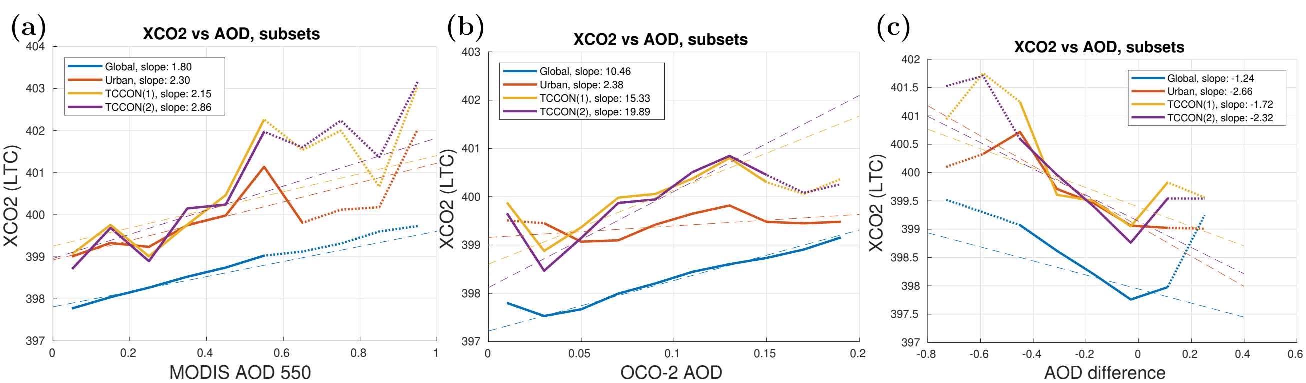


**Figure 9.** Dependence of bin-averaged $XCO_2$ (linear trend corrected, quality filtered) on AOD for three subsets of OCO-2 data and TCCON (solid lines). **a)** $XCO_2$ vs MODIS AOD. **b)** $XCO_2$ vs OCO-2 total AOD. **c)** $XCO_2$ vs AOD difference (OCO-2 - MODIS). The dashed lines show simple linear regression lines. The dotted parts of the bin-average lines correspond to AOD bins with less than 1% of all data.

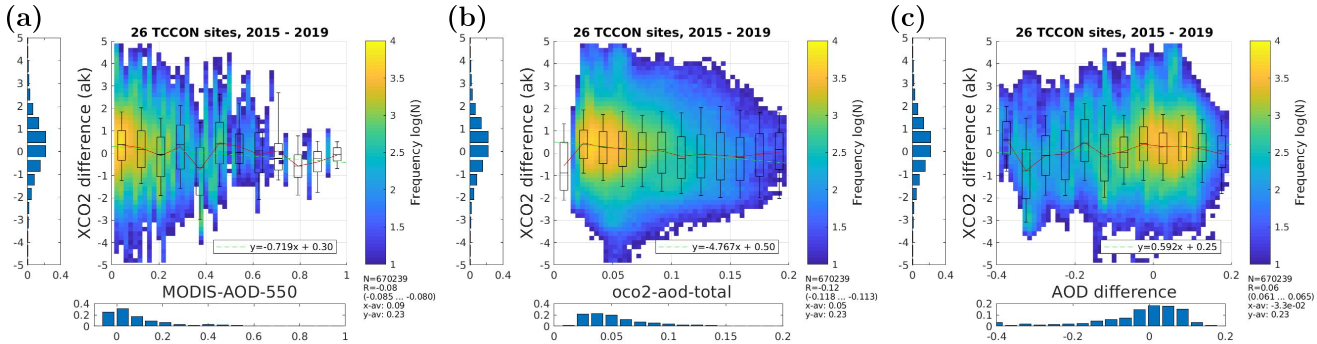


**Figure 10.** $XCO_2$ vs AOD for collocated quality filtered TCCON/OCO-2/MODIS dataset (2015-2019). $XCO_2$ value from TCCON (ttccon-match-60min) is aggregated for one hour time window centered at the OCO-2 overpass time. $XCO_2$ difference is OCO-2 minus TCCON, AOD difference is OCO-2 minus MODIS.

## 4.4 Alternative AOD thresholds in anticipation of the CO2M

Satellite $XCO_2$ retrievals are known to have higher uncertainty in high aerosol conditions (Connor et al., 2016; O'Dell et al., 2018). Setting an AOD threshold for good quality retrievals is always a trade-off between coverage and quality of the data. While for OCO-2 a strict AOD threshold is used to ensure good quality retrievals, for the coming CO2M a good coverage over polluted regions is also crucial for monitoring $CO_2$ emissions. In the latter case it is also important to avoid possible sampling bias caused by excluding high AOD areas from analysis, considering the co-emission of anthropogenic aerosols and $CO_2$. The CO2M mission will include a dedicated aerosol instrument, the Multi-Angle Polarimeter (MAP), and is expected to be better equipped to deal with high aerosol conditions. In the upcoming CO2M mission the required AOD threshold for good quality retrievals is designed to be 0.5 (ESA, last access: 23 April 2024). In this section we estimate how the selected AOD threshold affects the coverage of satellite $XCO_2$ retrievals, in particular in urban areas with high co-emission of aerosols and $CO_2$.

Here we use the collocated, quality filtered OCO-2/MODIS dataset as a proxy for CO2M data. This dataset includes high MODIS AOD pixels, although the OCO-2 quality filter including an AOD threshold of 0.2 has been applied. We assume that the OCO-2 quality filtering assures that the $XCO_2$ data is of good quality even for higher MODIS AOD cases, as CO2M data is expected to be up to AOD of 0.5. This assumption is supported by a comparison of quality filtered OCO-2 $XCO_2$ data against TCCON, where additional collocated MODIS AOD thresholds had minimal effect on the retrieval quality (not shown). We further assume that the MODIS AOD in the collocated dataset is representative of 'true' AOD and can be used to study the AOD threshold, even though the OCO-2 quality filtering has removed a large part of the original pixels. With this collocated dataset, we can test what is the effect of relaxing MODIS AOD threshold from 0.2 to 0.5. We emphasise that this does not mean that we extend the OCO-2 coverage (or propose to relax the OCO-2 AOD threshold); the MODIS AOD threshold used here is an additional constraint on the quality filtered OCO-2 data.

Table 4 shows the fraction of collocated quality filtered data for two different MODIS AOD bins, using either 0.2 or 0.5 as the threshold for maximum AOD (at 550 nm). For the global dataset relaxing the MODIS AOD threshold from 0.2 to 0.5 increases the fraction of acceptable data by 14.4 percentage points, while the average $XCO_2$ is increased by 0.08 ppm. For the urban areas the increase in coverage is as high as 30.8 percentage points while the increase in $XCO_2$ is 0.14 ppm. This finding support the idea that being able to perform reliable $XCO_2$ retrievals at higher aerosol loads is crucial for capturing the anthropogenic $CO_2$ emissions.

Figure 11 shows the fraction of data in the two considered MODIS AOD bins zoomed-in to South-East Asia which stands out as high AOD area. Here the two MODIS AOD bins are partly overlapping, M1: -0.2 - 0.2 and M2: -0.2 - 0.5. M1 contains 59% of the data, while M2 contains 94% of the data in this area. We see that large areas have a low fraction of data in M1, while for M2 only a few heavy AOD areas have low fraction of data within the bin. The high values over India and Eastern China indicate that in these areas relaxing the MODIS AOD threshold from 0.2 to 0.5 increases the fraction of acceptable data considerably.

In conclusion, here we have used the quality filtered OCO-2 data as a proxy of the coming CO2M data, which can be further filtered by using AOD thresholds from collocated MODIS data. We find that if CO2M can handle AODs up to 0.5, this will significantly increase the coverage, in particular in the urban areas, compared to a case where AOD only up to 0.2 could be allowed. We also find that due to the correlation found between AOD and $XCO_2$, including data with higher AOD increases the mean $XCO_2$ values, especially for the urban pixels.

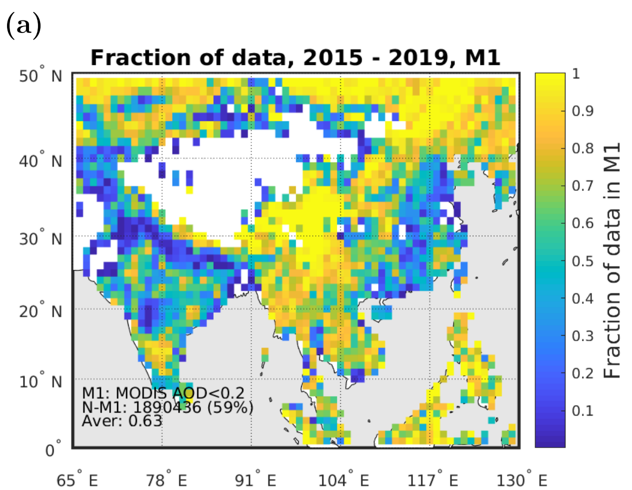


**Figure 11.** Difference in using MODIS AOD threshold 0.2 or 0.5 in Asia. Panels a) and b) show the fraction of data in M1 or M2, respectively, for each $1^\circ \times 1^\circ$ grid cell.

| Dataset | Fraction of data [%] | | | $XCO_2$ [ppm] | | |
|---|---|---|---|---|---|---|
| | AOD<0.2 | AOD<0.5 | $\Delta$ | AOD<0.2 | AOD<0.5 | $\Delta$ |
| Global | 84.0 | 98.3 | 14.4 | 397.9 | 397.9 | 0.08 |
| Urban | 63.8 | 94.6 | 30.8 | 399.1 | 399.3 | 0.14 |
| TCCON (1) | 83.5 | 98.1 | 14.6 | 399.4 | 399.4 | 0.03 |
| TCCON (2) | 83.5 | 98.1 | 14.6 | 399.1 | 399.2 | 0.07 |

**Table 4.** Difference between using 0.2 or 0.5 as MODIS AOD threshold (quality filtered data).

## 5 Conclusions

In this work, we have compiled and analysed a five-year dataset of co-located aerosol and $XCO_2$ satellite observations from MODIS/Aqua and OCO-2, focusing on the relationships between aerosols, $XCO_2$ retrieval quality, and data coverage in polluted areas. The primary aim was to understand how aerosols influence $XCO_2$ retrievals and how quality filtering decisions impact data availability and quality, particularly in urban regions with high emissions. We have shown that the total AOD value in ACOS full physics retrieval differs considerably from the MODIS Dark Target AOD over land for a large fraction of the data. The observed difference depends on location and conditions, but on average OCO-2 tends to overestimate at low aerosol loads and underestimate at higher AODs. This discrepancy highlights potential limitations in OCO-2 aerosol modeling that could influence $XCO_2$ retrievals. We found that the AOD difference is connected to the retrieved $XCO_2$ in the unfiltered dataset: $XCO_2$ values are lower when OCO-2 overestimates AOD and higher when AOD is underestimated.

We have found evidence of covariance of AOD and $XCO_2$, partly reflecting co-emission of anthropogenic $CO_2$ and aerosols from anthropogenic sources. A comparison with TCCON revealed a weak but statistically significant dependence of the $XCO_2$ bias on the AOD, such that at high AOD OCO-2 tends to underestimate $XCO_2$. This aerosol bias acts in the opposite direction than the observed covariance between AOD and $XCO_2$, partly masking the correlation.

The observed correlation between AOD and $XCO_2$ means that removing data under high AOD conditions not only excludes regions with elevated aerosol loads but also disproportionately removes observations of high $XCO_2$. The current OCO-2 quality filtering, which excludes data with AOD > 0.2, effectively mitigates retrieval errors associated with aerosol effects but at the cost of reduced coverage in polluted regions. These regions, such as urban areas with elevated $CO_2$ emissions, are critical for understanding anthropogenic contributions. Relaxing the AOD threshold to 0.5 increased the number of accepted data points globally by 14.4 percentage points, with a substantial improvement of 30.8 percentage points over urban areas. This adjustment would enable more comprehensive sampling of high-emission areas, especially in regions like Asia, where constant elevated aerosol loads often lead to significant data loss.

The correlation between AOD and $XCO_2$, combined with the observed $XCO_2$ bias at high AOD, underscores the challenge of separating real atmospheric covariance from retrieval artifacts. While our study does not directly link OCO-2 AOD underestimation to the observed $XCO_2$ bias, these results highlight the critical need to refine aerosol handling in future $XCO_2$ retrieval algorithms, particularly in polluted regions. The focus in this paper has been on the global multiyear statistics of AOD and $XCO_2$ in the collocated satellite dataset. The comparison with ground-based TCCON data has been done only statistically, combining all sites, to give a first reference point to independent data. Future work should focus on detailed site-specific studies, including comparisons with ground-based TCCON data, to disentangle retrieval biases from real atmospheric correlations.

Relaxing AOD thresholds could mitigate the significant sampling bias observed in high-emission regions but requires careful calibration to balance data quality and coverage. The upcoming CO2M mission, with its dedicated aerosol instrument and higher AOD threshold, represents a key opportunity to address these challenges and to ensure that observations provide robust support for the Global Stocktake and other climate initiatives.

*Code and data availability.* TEXT

The AERONET data is available from NASA Goddard Space Flight Center at https://aeronet.gsfc.nasa.gov/new_web/data.html. The TCCON data were obtained from the TCCON Data Archive hosted by CaltechDATA at https://tccondata.org (see Table A4 for references). The MODIS data used in this work can be found and downloaded using the NASA Earthdata Search website at https://www.earthdata.nasa.gov/. The OCO-2 data were produced by the OCO-2 project at the Jet Propulsion Laboratory, California Institute of Technology, and obtained from the OCO-2 data archive maintained at the NASA Goddard Earth Science Data and Information Services Center (OCO-2 Science Team et al., 2020). The collocated OCO-2/MODIS dataset created in this work and related codes are available as open data (Virtanen, 2024).

# Appendix A: Supplementary data

## A1 Supplementary Tables

## A2 Supplementary Figures

*Author contributions.* TEXT

TV, HL and AS conceptualized the study. AL did initial MODIS data processing. TV did most of the data processing and visualization. HL did the OCO-2/TCCON data collocation and OCO-2 anomaly data calculations. RN did data and image processing for the collocated AERONET/OCO-2 data. First draft of the manuscript was written by TV and HL. All authors contributed to editing the final version of the manuscript.

*Competing interests.* TEXT

The authors declare that they have no conflict of interest.

| Year | | | | All data (unfiltered) | | | | Good quality (Filtered) | | | |
|---|---|---|---|---|---|---|---|---|---|---|---|
| | OCO2 | Fraction | | AOD | | | $XCO_2$ | AOD | | | $XCO_2$ |
| | N [$10^6$] | MOD | QF | MOD | OCO2 | R | [ppm] | MOD | OCO2 | R | [ppm] |
| 2015 | 52.2M | 16.3 | 56.2 | 0.15 | 0.12 | 0.54 | 398.3 | 0.08 | 0.07 | 0.54 | 398.5 |
| 2016 | 67.1M | 13.6 | 57.2 | 0.15 | 0.11 | 0.64 | 401.6 | 0.08 | 0.07 | 0.53 | 401.8 |
| 2017 | 55.4M | 13.1 | 57.7 | 0.14 | 0.12 | 0.62 | 404.4 | 0.08 | 0.07 | 0.52 | 404.5 |
| 2018 | 66.9M | 13.6 | 56.4 | 0.15 | 0.12 | 0.63 | 406.0 | 0.09 | 0.07 | 0.52 | 406.2 |
| 2019 | 66.4M | 13.1 | 52.0 | 0.15 | 0.12 | 0.61 | 408.8 | 0.08 | 0.07 | 0.50 | 409.2 |
| Total | 308.0M | 13.9 | 55.9 | 0.15 | 0.12 | 0.60 | 403.8 | 0.08 | 0.07 | 0.52 | 404.0 |

**Table A1.** Number of data and average AOD and $XCO_2$ values for the five years of collocated OCO-2 and MODIS DT-land data considered in this work. Second column ('OCO2') shows the number of original OCO-2 data (in millions) for each year. The next column ('MOD') shows the fraction of OCO-2 data which have a matching MODIS AOD observation. The fourth column ('QF') shows the fraction of collocated data after OCO-2 quality filter has been applied (with respect to all collocated data). Also shown are the yearly average OCO-2 $XCO_2$ value and AOD value for each instrument, and the correlation coefficient (R) between the collocated AOD data for the unfiltered and filtered data, respectively.

| Not filtered | Fraction of data | | | | $\Delta XCO_2$ (ref: 398.1) [ppm] | | | | AOD | | | |
|---|---|---|---|---|---|---|---|---|---|---|---|---|
| **Dataset** | **Q1** | **Q2** | **Q3** | **Q4** | **Q1** | **Q2** | **Q3** | **Q4** | **MOD** | **OCO-2** | **R** | **N** |
| Global | 68.5 | 16.5 | 10.8 | 4.1 | -0.37 | 0.25 | 0.22 | -1.46 | 0.15 | 0.12 | 0.60 | 42.7M |
| Urban | 52.9 | 34.2 | 11.5 | 1.5 | 0.88 | 1.70 | 0.77 | -2.74 | 0.24 | 0.11 | 0.63 | 876k |
| TCCON(1) | 77.0 | 17.9 | 3.2 | 1.9 | 1.11 | 1.52 | 1.85 | -1.18 | 0.12 | 0.08 | 0.51 | 1.0M |
| TCCON(2) | 77.0 | 17.9 | 3.2 | 1.9 | 1.02 | 1.88 | 2.55 | 0.77 | 0.12 | 0.08 | 0.51 | 1.0M |

**Table A2.** $XCO_2$ statistics in different datasets without OCO-2 quality filtering. For TCCON collocation $XCO_2$ is obtained from OCO-2 (1) and TCCON (2). Anomaly data is not available for the unfiltered case, instead $\Delta XCO_2$ is calculated with respect to the reference value 398.1 ppm (the total global average value for good quality data). Linear trend correction (LTC) has been applied. p-values $< 10^{-6}$ for all cases.

*Acknowledgements.* We thank the AERONET PIs and their staff for establishing and maintaining the sites used in this investigation. We thank the PIs and others operating the TCCON sites for providing the data (Table A4). We thank the MODIS and OCO-2 science teams for the data used in this study. This work was supported by the Research Council of Finland (projects 331829, 337552, 353082, and 359196). Part of this work was carried out at the Jet Propulsion Laboratory, California Institute of Technology, under contract to the National Aeronautics and Space Administration (80NM0018D0004).

| | $XCO_2$ vs MODIS AOD | | $XCO_2$ vs OCO-2 AOD | | $XCO_2$ vs AOD difference | | AOD vs AOD | |
|---|---|---|---|---|---|---|---|---|
| **Dataset** | **R** | **Slope** | **R** | **Slope** | **R** | **Slope** | **R** | **Slope** |
| Global | 0.10 | 1.80 | 0.16 | 10.46 | -0.06 | -1.24 | 0.52 | 0.18 |
| Urban | 0.16 | 2.30 | 0.04 | 2.38 | -0.17 | -2.66 | 0.52 | 0.12 |
| TCCON(1) | 0.12 | 2.15 | 0.18 | 15.33 | -0.09 | -1.72 | 0.45 | 0.12 |
| TCCON(2) | 0.17 | 2.86 | 0.25 | 19.89 | -0.13 | -2.32 | 0.45 | 0.12 |

**Table A3.** Statistics for correlation between AOD and $XCO_2$ and bivariate linear regression slopes for different subsets of the quality filtered collocated MODIS/OCO-2 five year (2015-2019) dataset. The first three slopes (columns 3, 5, and 7) are for $XCO_2$ as function of AOD (or AOD difference), while the last column gives the fitted slope for OCO-2 AOD as function of MODIS AOD. p-values are smaller than $10^{-6}$ for all cases.

## References


Blumenstock, T., Hase, F., Schneider, M., García, O., and Sepúlveda, E.: TCCON data from Izana, Tenerife, Spain, Release GGG2020R0. TCCON data archive, hosted by CaltechDATA, California Institute of Technology, Pasadena, CA, U.S.A., https://doi.org/10.14291/tccon.ggg2020.izana01.R1, 2017.

Buschmann, M., Petri, C., Palm, M., Warneke, T., Notholt, J., and Engineers, A. S.: TCCON data from Ny-Alesund, Svalbard, Norway, Release GGG2020R0. TCCON data archive, hosted by CaltechDATA, California Institute of Technology, Pasadena, CA, U.S.A., https://doi.org/10.14291/tccon.ggg2020.nyalesund01.R0, 2022.

Butz, A., Hasekamp, O. P., Frankenberg, C., and Aben, I.: Retrievals of atmospheric CO 2 from simulated space-borne measurements of backscattered near-infrared sunlight: accounting for aerosol effects, Applied optics, 48, 3322–3336, 2009.

Connor, B., Bösch, H., McDuffie, J., Taylor, T., Fu, D., Frankenberg, C., O'Dell, C., Payne, V. H., Gunson, M., Pollock, R., et al.: Quantification of uncertainties in OCO-2 measurements of XCO 2: Simulations and linear error analysis, Atmospheric Measurement Techniques, 9, 5227–5238, 2016.

Crisp, D., Atlas, R. M., Breon, F.-M., Brown, L., Burrows, J., Ciais, P., Connor, B., Doney, S., Fung, I., Jacob, D., et al.: The orbiting carbon observatory (OCO) mission, Advances in Space Research, 34, 700–709, 2004.

Crisp, D., O'Dell, C., Eldering, A., Fisher, B., Oyafuso, F., Payne, V., Drouin, B., Toon, G., Laughner, J., Somkuti, P., McGarragh, G., Merrelli, A., Nelson, R., Gunson, M., Frankenberg, C., Osterman, G., Boesch, H., Brown, L., Castano, R., Christi, M., Connor, B., McDuffie, J., Miller, C., Natraj, V., O'Brien, D., Polonski, I., Smyth, M., Thompson, D., and Granat, R.: Orbiting Carbon Observatory-2 & 3 (OCO-2 & OCO-3) Level 2 Full Physics Retrieval Algorithm Theoretical Basis, https://docserver.gesdisc.eosdis.nasa.gov/public/project/OCO/OCO_L2_ATBD.pdf, 2021.

Crowell, S., Baker, D., Schuh, A., Basu, S., Jacobson, A. R., Chevallier, F., Liu, J., Deng, F., Feng, L., McKain, K., et al.: The 2015–2016 carbon cycle as seen from OCO-2 and the global in situ network, Atmospheric Chemistry and Physics, 19, 9797–9831, 2019.

Dubey, M., Henderson, B., Green, D., Butterfield, Z., Keppel-Aleks, G., Allen, N., Blavier, J.-F., Roehl, C., Wunch, D., and Lindenmaier, R.: TCCON data from Manaus, Brazil, Release GGG2020R0. TCCON data archive, hosted by CaltechDATA, California Institute of Technology, Pasadena, CA, U.S.A., https://doi.org/10.14291/tccon.ggg2020.manaus01.R0, 2022.

| Site Name | Location | Data Citation |
|---|---|---|
| bremen01 | Bremen, Germany | Notholt et al. (2022) |
| burgos01 | Burgos, Philippines | Morino et al. (2022c) |
| pasadena01 | Pasadena, California, USA | Wennberg et al. (2022c) |
| easttroutlake01 | East Trout Lake, Canada | Wunch et al. (2022) |
| edwards01 | AFRC, Edwards, CA, USA | Iraci et al. (2022b) |
| eureka01 | Eureka, Canada | Strong et al. (2022) |
| garmisch01 | Garmisch, Germany | Sussmann and Rettinger (2017) |
| indianapolis01 | Indianapolis, Indiana, USA | Iraci et al. (2022a) |
| izana01 | Izana, Tenerife, Spain | Blumenstock et al. (2017) |
| jpl02 | JPL, Pasadena, California, USA | Wennberg et al. (2022a) |
| saga01 | Saga, Japan | Shiomi et al. (2022) |
| karlsruhe01 | Karlsruhe, Germany | Hase et al. (2022) |
| lauder02 | Lauder, New Zealand | Sherlock et al. (2022) |
| lauder03 | Lauder, New Zealand | Pollard et al. (2022) |
| manaus01 | Manaus, Brazil | Dubey et al. (2022) |
| nicosia01 | Nicosia, Cyprus | Petri et al. (2023) |
| nyalesund01 | Ny-Ålesund, Svalbard, Norway | Buschmann et al. (2022) |
| lamont01 | Lamont, Oklahoma, USA | Wennberg et al. (2022d) |
| orleans01 | Orleans, France | Warneke et al. (2022) |
| parkfalls01 | Park Falls, Wisconsin, USA | Wennberg et al. (2022b) |
| paris01 | Sorbonne Université, Paris, FR | Te et al. (2022) |
| reunion01 | Reunion Island, France | Maziere et al. (2022) |
| rikubetsu01 | Rikubetsu, Hokkaido, Japan | Morino et al. (2022a) |
| sodankyla01 | Sodankylä, Finland | Kivi et al. (2022) |
| tsukuba02 | Tsukuba, Ibaraki, Japan, 125HR | Morino et al. (2022b) |
| xianghe01 | Xianghe, China | Zhou et al. (2022) |

**Table A4.** 26 TCCON sites used in this study.

Eck, T. F., Holben, B. N., Reid, J. S., Dubovik, O., Smirnov, A., O'Neill, N. T., Slutsker, I., and Kinne, S.: Wavelength dependence of the optical depth of biomass burning, urban, and desert dust aerosols, Journal of Geophysical Research, 104, 31 333–31 349, https://doi.org/https://doi.org/10.1029/1999JD900923, 1999.

ESA: Copernicus CO2 monitoring mission requirements document (MRD). Tech. rep. Version 3.0, https://esamultimedia.esa.int/docs/EarthObservation/CO2M_MRD_v3.0_20201001_Issued.pdf, last access: 23 April 2024.

Giles, D. M., Sinyuk, A., Sorokin, M. G., Schafer, J. S., Smirnov, A., Slutsker, I., Eck, T. F., Holben, B. N., Lewis, J. R., Campbell, J. R., Welton, E. J., Korkin, S. V., and Lyapustin, A. I.: Advancements in the Aerosol Robotic Network (AERONET) Version 3 database

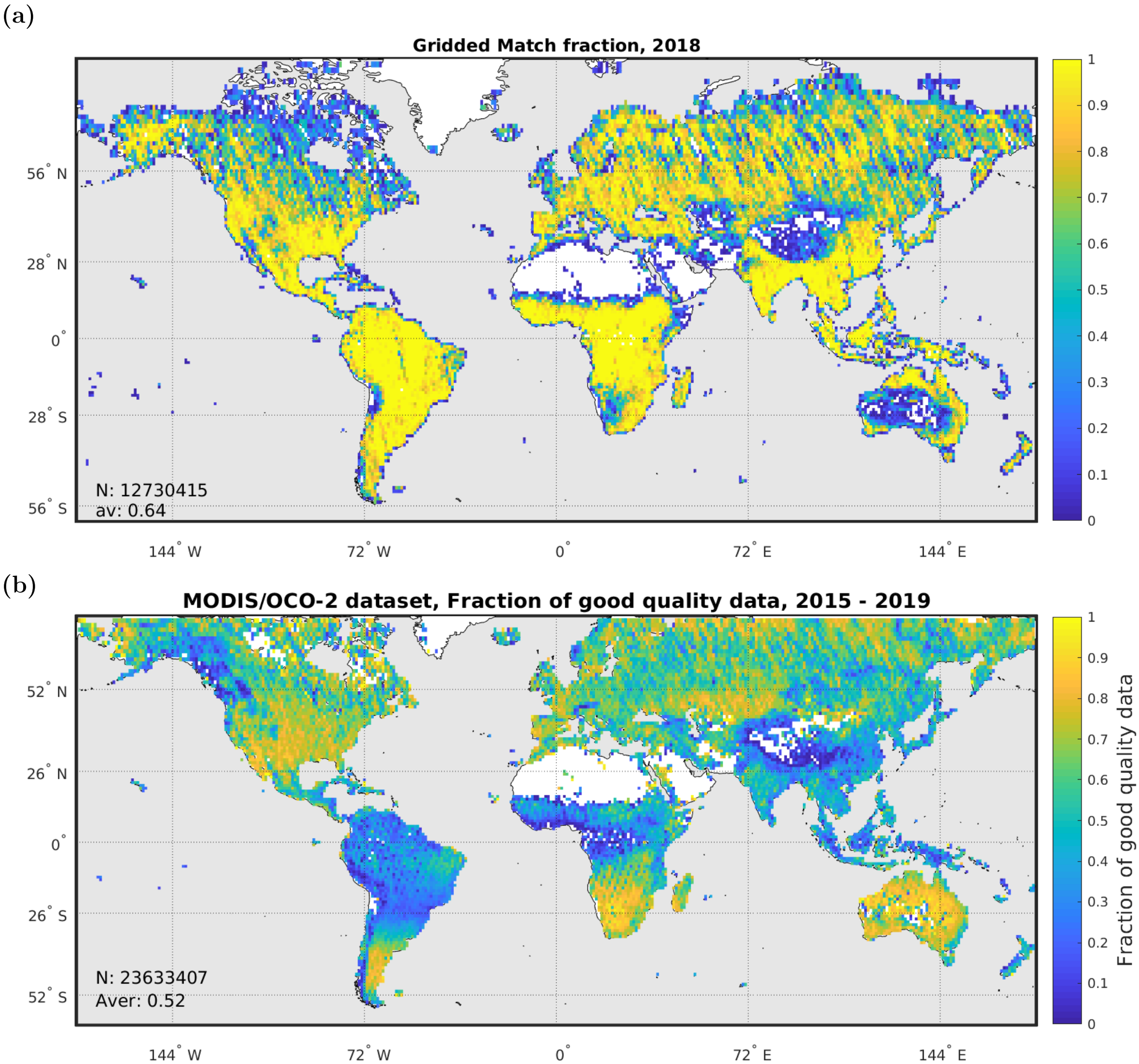


**Figure A1. a)** Fraction of OCO-2 datapoints (without quality filtering) with matching MODIS data for $1^\circ \times 1^\circ$ grid cells. The fraction is only shown for grid cells which have at least one MODIS data point. $N$ means total number of MODIS data points. The average fraction (64%) of OCO-2 data points with matching MODIS data is calculated over those grid cells, which have non-zero fraction. Example for one year, 2018. **b)** Fraction of good quality data for each $1^\circ \times 1^\circ$ grid cell in the collocated MODIS/OCO-2 dataset.

– automated near-real-time quality control algorithm with improved cloud screening for Sun photometer aerosol optical depth (AOD) measurements, Atmospheric Measurement Techniques, 12, 169–209, https://doi.org/10.5194/amt-12-169-2019, 2019.

Global Modeling And Assimilation Office: MERRA-2 tavgM_2d_aer_Nx: 2d,Monthly mean,Time-averaged,Single-Level,Assimilation,Aerosol Diagnostics V5.12.4, https://doi.org/10.5067/FH9A0MLJPC7N, last access: 22 April 2024.

Guerlet, S., Butz, A., Schepers, D., Basu, S., Hasekamp, O., Kuze, A., Yokota, T., Blavier, J.-F., Deutscher, N., Griffith, D. T., et al.: Impact of aerosol and thin cirrus on retrieving and validating XCO2 from GOSAT shortwave infrared measurements, Journal of Geophysical Research: Atmospheres, 118, 4887–4905, 2013.

Gupta, P., Levy, R. C., Mattoo, S., Remer, L. A., and Munchak, L. A.: A surface reflectance scheme for retrieving aerosol optical depth over urban surfaces in MODIS Dark Target retrieval algorithm, Atmospheric Measurement Techniques, 9, 3293–3308, https://doi.org/10.5194/amt-9-3293-2016, 2016.

Gupta, P., Remer, L. A., Levy, R. C., and Mattoo, S.: Validation of MODIS 3 km land aerosol optical depth from NASA's EOS Terra and Aqua missions, Atmospheric Measurement Techniques, 11, 3145–3159, https://doi.org/10.5194/amt-11-3145-2018, 2018.

Hase, F., Blumenstock, T., Dohe, S., Gro{\ss}, J., and Kiel, M.: TCCON data from Karlsruhe, Germany, Release GGG2020R1. TCCON data archive, hosted by CaltechDATA, California Institute of Technology, Pasadena, CA, U.S.A., https://doi.org/10.14291/tccon.ggg2020.karlsruhe01.R1, 2022.

He, Q., Zhang, M., Huang, B., and Tong, X.: MODIS 3 km and 10 km aerosol optical depth for China: Evaluation and comparison, Atmospheric Environment, 153, 150–162, https://doi.org/https://doi.org/10.1016/j.atmosenv.2017.01.023, 2017.

Holben, B., Eck, T., Slutsker, I., Tanré, D., Buis, J., Setzer, A., Vermote, E., Reagan, J., Kaufman, Y., Nakajima, T., Lavenu, F., Jankowiak, I., and Smirnov, A.: AERONET—A Federated Instrument Network and Data Archive for Aerosol Characterization, Remote Sensing of Environment, 66, 1–16, https://doi.org/https://doi.org/10.1016/S0034-4257(98)00031-5, 1998.

Houweling, S., Baker, D., Basu, S., Boesch, H., Butz, A., Chevallier, F., Deng, F., Dlugokencky, E., Feng, L., Ganshin, A., et al.: An intercomparison of inverse models for estimating sources and sinks of CO2 using GOSAT measurements, Journal of Geophysical Research: Atmospheres, 120, 5253–5266, 2015.

Hsu, N., Tsay, S.-C., King, M., and Herman, J.: Aerosol properties over bright-reflecting source regions, IEEE Transactions on Geoscience and Remote Sensing, 42, 557–569, https://doi.org/10.1109/TGRS.2004.824067, 2004.

https://ladsweb.modaps.eosdis.nasa.gov: NASA Level-1 and Atmosphere Archive Distribution System Distributed Active Archive Center, https://ladsweb.modaps.eosdis.nasa.gov/, last access: 14 November 2024.

Iraci, L., Podolske, J., Hillyard, P., Roehl, C., Wennberg, P. O., Blavier, J.-F., Landeros, J., Allen, N., Wunch, D., Zavaleta, J., Quigley, E., Osterman, G., Barrow, E., and Barney, J.: TCCON data from Indianapolis, Indiana, USA, Release GGG2020R0. TCCON data archive, hosted by CaltechDATA, California Institute of Technology, Pasadena, CA, U.S.A., https://doi.org/10.14291/tccon.ggg2020.indianapolis01.R1, 2022a.

Iraci, L., Podolske, J., Roehl, C., Wennberg, P. O., Blavier, J.-F., Allen, N., Wunch, D., and Osterman, G.: TCCON data from Armstrong Flight Research Center, Edwards, CA, USA, Release GGG2020R0. TCCON data archive, hosted by CaltechDATA, California Institute of Technology, Pasadena, CA, U.S.A., https://doi.org/10.14291/tccon.ggg2020.edwards01.R0, 2022b.

Janssens-Maenhout, G., Pinty, B., Dowell, M., Zunker, H., Andersson, E., Balsamo, G., Bézy, J.-L., Brunhes, T., Bösch, H., Bojkov, B., et al.: Toward an operational anthropogenic CO 2 emissions monitoring and verification support capacity, Bulletin of the American Meteorological Society, 101, E1439–E1451, 2020.

Kivi, R., Heikkinen, P., and Kyro, E.: TCCON data from Sodankyla, Finland, Release GGG2020R0. TCCON data archive, hosted by CaltechDATA, California Institute of Technology, Pasadena, CA, U.S.A., https://doi.org/10.14291/tccon.ggg2020.sodankyla01.R0, 2022.

Lamminpää, O., Hobbs, J., Brynjarsdóttir, J., Laine, M., Braverman, A., Lindqvist, H., and Tamminen, J.: Accelerated MCMC for satellite-based measurements of atmospheric CO2, Remote Sensing, 11, 2061, 2019.

Laughner, J. L., Toon, G. C., Mendonca, J., Petri, C., Roche, S., Wunch, D., Blavier, J.-F., Griffith, D. W. T., Heikkinen, P., Keeling, R. F., Kiel, M., Kivi, R., Roehl, C. M., Stephens, B. B., Baier, B. C., Chen, H., Choi, Y., Deutscher, N. M., DiGangi, J. P., Gross, J., Herkommer, B., Jeseck, P., Laemmel, T., Lan, X., McGee, E., McKain, K., Miller, J., Morino, I., Notholt, J., Ohyama, H., Pollard, D. F., Rettinger, M., Riris, H., Rousogenous, C., Sha, M. K., Shiomi, K., Strong, K., Sussmann, R., Té, Y., Velazco, V. A., Wofsy, S. C., Zhou, M., and Wennberg, P. O.: The Total Carbon Column Observing Network's GGG2020 data version, Earth System Science Data, 16, 2197–2260, https://doi.org/10.5194/essd-16-2197-2024, 2024.

Levy, R. and Hsu, C., e. a.: MODIS Atmosphere L2 Aerosol Product, https://doi.org/http://dx.doi.org/10.5067/MODIS/MYD04_L2.006, 2015.

Levy, R. C., Remer, L. A., Kleidman, R. G., Mattoo, S., Ichoku, C., Kahn, R., and Eck, T. F.: Global evaluation of the Collection 5 MODIS dark-target aerosol products over land, Atmospheric Chemistry and Physics, 10, 10 399–10 420, https://doi.org/10.5194/acp-10-10399-2010, 2010.

Levy, R. C., Mattoo, S., Munchak, L. A., Remer, L. A., Sayer, A. M., Patadia, F., and Hsu, N. C.: The Collection 6 MODIS aerosol products over land and ocean, Atmospheric Measurement Techniques, 6, 2989–3034, https://doi.org/10.5194/amt-6-2989-2013, 2013.

Lindqvist, H., O'Dell, C. W., Basu, S., Boesch, H., Chevallier, F., Deutscher, N., Feng, L., Fisher, B., Hase, F., Inoue, M., Kivi, R., Morino, I., Palmer, P. I., Parker, R., Schneider, M., Sussmann, R., and Yoshida, Y.: Does GOSAT capture the true seasonal cycle of carbon dioxide?, Atmospheric Chemistry and Physics, 15, 13 023–13 040, https://doi.org/10.5194/acp-15-13023-2015, 2015.

Maziere, D., M., M. K. S., Desmet, F., Hermans, C., Scolas, F., Kumps, N., Zhou, M., Metzger, J.-M., Duflot, V., and Cammas, J.-P.: TCCON data from Reunion Island (La Reunion), France, Release GGG2020R0. TCCON data archive, hosted by CaltechDATA, California Institute of Technology, Pasadena, CA, U.S.A., https://doi.org/10.14291/tccon.ggg2020.reunion01.R0, 2022.

Meijer, Y., Andersson, E., Boesch, H., Dubovik, O., Houweling, S., Landgraf, J., Lang, R., and Lindqvist, H.: Editorial: Anthropogenic emission monitoring with the Copernicus CO2 monitoring mission, Frontiers in Remote Sensing, 4, https://doi.org/10.3389/frsen.2023.1217568, 2023.

Mendonca, J., Nassar, R., O'Dell, C. W., Kivi, R., Morino, I., Notholt, J., Petri, C., Strong, K., and Wunch, D.: Assessing the feasibility of using a neural network to filter Orbiting Carbon Observatory 2 (OCO-2) retrievals at northern high latitudes, Atmospheric Measurement Techniques, 14, 7511–7524, 2021.

Morino, I., Ohyama, H., Hori, A., and Ikegami, H.: TCCON data from Rikubetsu, Hokkaido, Japan, Release GGG2020R0. TCCON data archive, hosted by CaltechDATA, California Institute of Technology, Pasadena, CA, U.S.A., https://doi.org/10.14291/tccon.ggg2020.rikubetsu01.R0, 2022a.

Morino, I., Ohyama, H., Hori, A., and Ikegami, H.: TCCON data from Tsukuba, Ibaraki, Japan, 125HR, Release GGG2020R0. TCCON data archive, hosted by CaltechDATA, California Institute of Technology, Pasadena, CA, U.S.A., https://doi.org/10.14291/tccon.ggg2020.tsukuba02.R0, 2022b.

Morino, I., Velazco, V. A., Hori, A., Uchino, O., and Griffith, D. W. T.: TCCON data from Burgos, Philippines, Release GGG2020R0. TCCON data archive, hosted by CaltechDATA, California Institute of Technology, Pasadena, CA, U.S.A., https://doi.org/10.14291/tccon.ggg2020.burgos01.R0, 2022c.

NaturalEarth: Urban Areas, https://www.naturalearthdata.com/downloads/50m-cultural-vectors/50m-urban-areas/, last access: 22 April 2024.

NOAA Global Monitoring Laboratory: Trends in Atmospheric Carbon Dioxide, https://gml.noaa.gov/ccgg/trends/gl_gr.html, last access: 22 April 2024.

Notholt, J., Petri, C., Warneke, T., Deutscher, N., Buschmann, M., Weinzierl, C., Macatangay, R., and Grupe, P.: TCCON data from Bremen, Germany, Release GGG2020R0. TCCON data archive, hosted by CaltechDATA, California Institute of Technology, Pasadena, CA, U.S.A., https://doi.org/10.14291/tccon.ggg2020.bremen01.R0, 2022.

OCO-2 Science Team, Gunson, M., and Eldering, A.: OCO-2 Level 2 bias-corrected XCO2 and other select fields from the full-physics retrieval aggregated as daily files, Retrospective processing V10r, https://doi.org/10.5067/E4E140XDMPO2, 2020.

O'Dell, C. W., Eldering, A., Wennberg, P. O., Crisp, D., Gunson, M. R., Fisher, B., Frankenberg, C., Kiel, M., Lindqvist, H., Mandrake, L., Merrelli, A., Natraj, V., Nelson, R. R., Osterman, G. B., Payne, V. H., Taylor, T. E., Wunch, D., Drouin, B. J., Oyafuso, F., Chang, A., McDuffie, J., Smyth, M., Baker, D. F., Basu, S., Chevallier, F., Crowell, S. M. R., Feng, L., Palmer, P. I., Dubey, M., García, O. E., Griffith, D. W. T., Hase, F., Iraci, L. T., Kivi, R., Morino, I., Notholt, J., Ohyama, H., Petri, C., Roehl, C. M., Sha, M. K., Strong, K., Sussmann, R., Te, Y., Uchino, O., and Velazco, V. A.: Improved retrievals of carbon dioxide from Orbiting Carbon Observatory-2 with the version 8 ACOS algorithm, Atmospheric Measurement Techniques, 11, 6539–6576, https://doi.org/10.5194/amt-11-6539-2018, 2018.

Petri, C., Vrekoussis, M., Rousogenous, C., Warneke, T., Sciare, J., and Notholt, J.: TCCON data from Nicosia, Cyprus, Release GGG2020R0. TCCON data archive, hosted by CaltechDATA, California Institute of Technology, Pasadena, CA, U.S.A., https://doi.org/10.14291/tccon.ggg2020.nicosia01.R0, 2023.

Pollard, D., Robinson, J., and Shiona, H.: TCCON data from Lauder, New Zealand, 125HR, Release GGG2020R0. TCCON data archive, hosted by CaltechDATA, California Institute of Technology, Pasadena, CA, U.S.A., https://doi.org/10.14291/tccon.ggg2020.lauder03.R0, 2022.

Remer, L. A., Mattoo, S., Levy, R. C., and Munchak, L. A.: MODIS 3 km aerosol product: algorithm and global perspective, Atmospheric Measurement Techniques, 6, 1829–1844, https://doi.org/10.5194/amt-6-1829-2013, 2013.

Rusli, S. P., Hasekamp, O., Fu, G., Meijer, Y., Landgraf, J., et al.: Anthropogenic CO 2 monitoring satellite mission: the need for multi-angle polarimetric observations, Atmospheric Measurement Techniques, 14, 1167–1190, 2021.

Sanghavi, S., Nelson, R., Frankenberg, C., and Gunson, M.: Aerosols in OCO-2/GOSAT retrievals of XCO2: An information content and error analysis, Remote Sensing of Environment, 251, 112 053, https://doi.org/https://doi.org/10.1016/j.rse.2020.112053, 2020.

Sayer, A. M., Munchak, L. A., Hsu, N. C., Levy, R. C., Bettenhausen, C., and Jeong, M.-J.: MODIS Collection 6 aerosol products: Comparison between Aqua's e-Deep Blue, Dark Target, and "merged" data sets, and usage recommendations, Journal of Geophysical Research: Atmospheres, 119, 13,965–13,989, https://doi.org/10.1002/2014jd022453, 2014.

Schneider, A., Friedl, M. A., and Potere, D.: A new map of global urban extent from MODIS satellite data, Environmental Research Letters, 4, 044 003, https://doi.org/10.1088/1748-9326/4/4/044003, 2009.

Sherlock, V., Connor, B., Robinson, J., Shiona, H., Smale, D., and Pollard, D.: TCCON data from Lauder, New Zealand, 125HR, Release GGG2020R0. TCCON data archive, hosted by CaltechDATA, California Institute of Technology, Pasadena, CA, U.S.A., https://doi.org/10.14291/tccon.ggg2020.lauder02.R0, 2022.

Shiomi, K., Kawakami, S., Ohyama, H., Arai, K., Okumura, H., Ikegami, H., and Usami, M.: TCCON data from Saga, Japan, Release GGG2020R0. TCCON data archive, hosted by CaltechDATA, California Institute of Technology, Pasadena, CA, U.S.A., https://doi.org/10.14291/tccon.ggg2020.saga01.R0, 2022.

Sinyuk, A., Holben, B. N., Eck, T. F., Giles, D. M., Slutsker, I., Korkin, S., Schafer, J. S., Smirnov, A., Sorokin, M., and Lyapustin, A.: The AERONET Version 3 aerosol retrieval algorithm, associated uncertainties and comparisons to Version 2, Atmospheric Measurement Techniques, 13, 3375–3411, https://doi.org/10.5194/amt-13-3375-2020, 2020.

Strong, K., Roche, S., Franklin, J., Mendonca, J., Lutsch, E., Weaver, D., Fogal, P., Drummond, J., Batchelor, R., and Lindenmaier, R.: TCCON data from Eureka, Canada, Release GGG2020R0. TCCON data archive, hosted by CaltechDATA, California Institute of Technology, Pasadena, CA, U.S.A., https://doi.org/10.14291/tccon.ggg2020.eureka01.R0, 2022.

Sussmann, R. and Rettinger, M.: TCCON data from Garmisch, Germany, Release GGG2020R0. TCCON data archive, hosted by CaltechDATA, California Institute of Technology, Pasadena, CA, U.S.A., https://doi.org/10.14291/tccon.ggg2020.garmisch01.R0, 2017.

Taylor, T. E., O'Dell, C. W., Baker, D., Bruegge, C., Chang, A., Chapsky, L., Chatterjee, A., Cheng, C., Chevallier, F., Crisp, D., Dang, L., Drouin, B., Eldering, A., Feng, L., Fisher, B., Fu, D., Gunson, M., Haemmerle, V., Keller, G. R., Kiel, M., Kuai, L., Kurosu, T., Lambert, A., Laughner, J., Lee, R., Liu, J., Mandrake, L., Marchetti, Y., McGarragh, G., Merrelli, A., Nelson, R. R., Osterman, G., Oyafuso, F., Palmer, P. I., Payne, V. H., Rosenberg, R., Somkuti, P., Spiers, G., To, C., Weir, B., Wennberg, P. O., Yu, S., and Zong, J.: Evaluating the consistency between OCO-2 and OCO-3 $XCO_2$ estimates derived from the NASA ACOS version 10 retrieval algorithm, Atmospheric Measurement Techniques, 16, 3173–3209, https://doi.org/10.5194/amt-16-3173-2023, 2023.

Te, Y., Jeseck, P., and Janssen, C.: TCCON data from Paris, France, Release GGG2020R0. TCCON data archive, hosted by CaltechDATA, California Institute of Technology, Pasadena, CA, U.S.A., https://doi.org/10.14291/tccon.ggg2020.paris01.R0, 2022.

Virtanen, T. H.: Data and code for manuscript "A global perspective on CO2 satellite observations in high AOD conditions" by Virtanen et al., https://doi.org/10.57707/FMI-B2SHARE.62269CB9CF944D5595692A5F8EA6B915, 2024.

Virtanen, T. H., Kolmonen, P., Sogacheva, L., Rodríguez, E., Saponaro, G., and de Leeuw, G.: Collocation mismatch uncertainties in satellite aerosol retrieval validation, Atmospheric Measurement Techniques, 11, 925–938, https://doi.org/10.5194/amt-11-925-2018, 2018.

Warneke, T., Messerschmidt, J., Notholt, J., Weinzierl, C., Deutscher, N., Petri, C., Grupe, P., Vuillemin, C., Truong, F., Schmidt, M., Ramonet, M., and Parmentier, E.: TCCON data from Orleans, France, Release GGG2020R0. TCCON data archive, hosted by CaltechDATA, California Institute of Technology, Pasadena, CA, U.S.A., https://doi.org/10.14291/tccon.ggg2020.orleans01.R0, 2022.

Wei, J., Li, Z., Peng, Y., and Sun, L.: MODIS Collection 6.1 aerosol optical depth products over land and ocean: validation and comparison, Atmospheric Environment, 201, 428–440, https://doi.org/https://doi.org/10.1016/j.atmosenv.2018.12.004, 2019.

Wennberg, P. O., Roehl, C., Blavier, J.-F., Wunch, D., Landeros, J., and Allen, N.: TCCON data from Jet Propulsion Laboratory, Pasadena, California, USA, Release GGG2020R0. TCCON data archive, hosted by CaltechDATA, California Institute of Technology, Pasadena, CA, U.S.A., https://doi.org/10.14291/tccon.ggg2020.jpl02.R0, 2022a.

Wennberg, P. O., Roehl, C., Wunch, D., Toon, G. C., Blavier, J.-F., Washenfelder, R., Keppel-Aleks, G., Allen, N., and Ayers, J.: TCCON data from Park Falls, Wisconsin, USA, Release GGG2020R1. TCCON data archive, hosted by CaltechDATA, California Institute of Technology, Pasadena, CA, U.S.A., https://doi.org/10.14291/tccon.ggg2020.parkfalls01.R1, 2022b.

Wennberg, P. O., Wunch, D., Roehl, C., Blavier, J.-F., Toon, G. C., and Allen, N.: TCCON data from California Institute of Technology, Pasadena, California, USA, Release GGG2020R0. TCCON data archive, hosted by CaltechDATA, California Institute of Technology, Pasadena, CA, U.S.A., https://doi.org/10.14291/tccon.ggg2020.pasadena01.R0, 2022c.

Wennberg, P. O., Wunch, D., Roehl, C., Blavier, J.-F., Toon, G. C., Allen, N., Dowell, P., Teske, K., Martin, C., and Martin, J.: TCCON data from Lamont, Oklahoma, USA, Release GGG2020R0. TCCON data archive, hosted by CaltechDATA, California Institute of Technology, Pasadena, CA, U.S.A., https://doi.org/10.14291/tccon.ggg2020.lamont01.R0, 2022d.

Wunch, D., Toon, G. C., Blavier, J.-F. L., Washenfelder, R., Notholt, J., Connor, B. J., Griffith, D. W. T., Sherlock, V., and Wennberg, P. O: The Total Carbon Column Observing Network, Philos. T. R. Soc. A, 369, 2087–2112, https://doi.org/https://doi.org/10.1098/rsta.2010.0240, 2011.

Wunch, D., Wennberg, P. O., Osterman, G., Fisher, B., Naylor, B., Roehl, C. M., O'Dell, C., Mandrake, L., Viatte, C., Kiel, M., Griffith, D. W. T., Deutscher, N. M., Velazco, V. A., Notholt, J., Warneke, T., Petri, C., De Maziere, M., Sha, M. K., Sussmann, R., Rettinger, M., Pollard, D., Robinson, J., Morino, I., Uchino, O., Hase, F., Blumenstock, T., Feist, D. G., Arnold, S. G., Strong, K., Mendonca, J., Kivi, R., Heikkinen, P., Iraci, L., Podolske, J., Hillyard, P. W., Kawakami, S., Dubey, M. K., Parker, H. A., Sepulveda, E., García, O. E., Te, Y., Jeseck, P., Gunson, M. R., Crisp, D., and Eldering, A.: Comparisons of the Orbiting Carbon Observatory-2 (OCO-2) $XCO_2$ measurements with TCCON, Atmospheric Measurement Techniques, 10, 2209–2238, https://doi.org/10.5194/amt-10-2209-2017, 2017.

Wunch, D., Mendonca, J., Colebatch, O., Allen, N., Blavier, J.-F. L., Kunz, K., Roche, S., Hedelius, J., Neufeld, G., Springett, S., Worthy, D., Kessler, R., and Strong, K.: TCCON data from East Trout Lake, Canada, Release GGG2020R0. TCCON data archive, hosted by CaltechDATA, California Institute of Technology, Pasadena, CA, U.S.A., https://doi.org/10.14291/tccon.ggg2020.easttroutlake01.R0, 2022.

Yang, D., Liu, Y., Cai, Z., Chen, X., Yao, L., and Lu, D.: First global carbon dioxide maps produced from TanSat measurements, 2018.

Yokota, T., Yoshida, Y., Eguchi, N., Ota, Y., Tanaka, T., Watanabe, H., and Maksyutov, S.: Global concentrations of CO2 and CH4 retrieved from GOSAT: First preliminary results, Sola, 5, 160–163, 2009.

Zhou, M., Wang, P., Nan, W., Yang, Y., Kumps, N., Hermans, C., and De Mazière, M.: TCCON data from Xianghe, 2022.

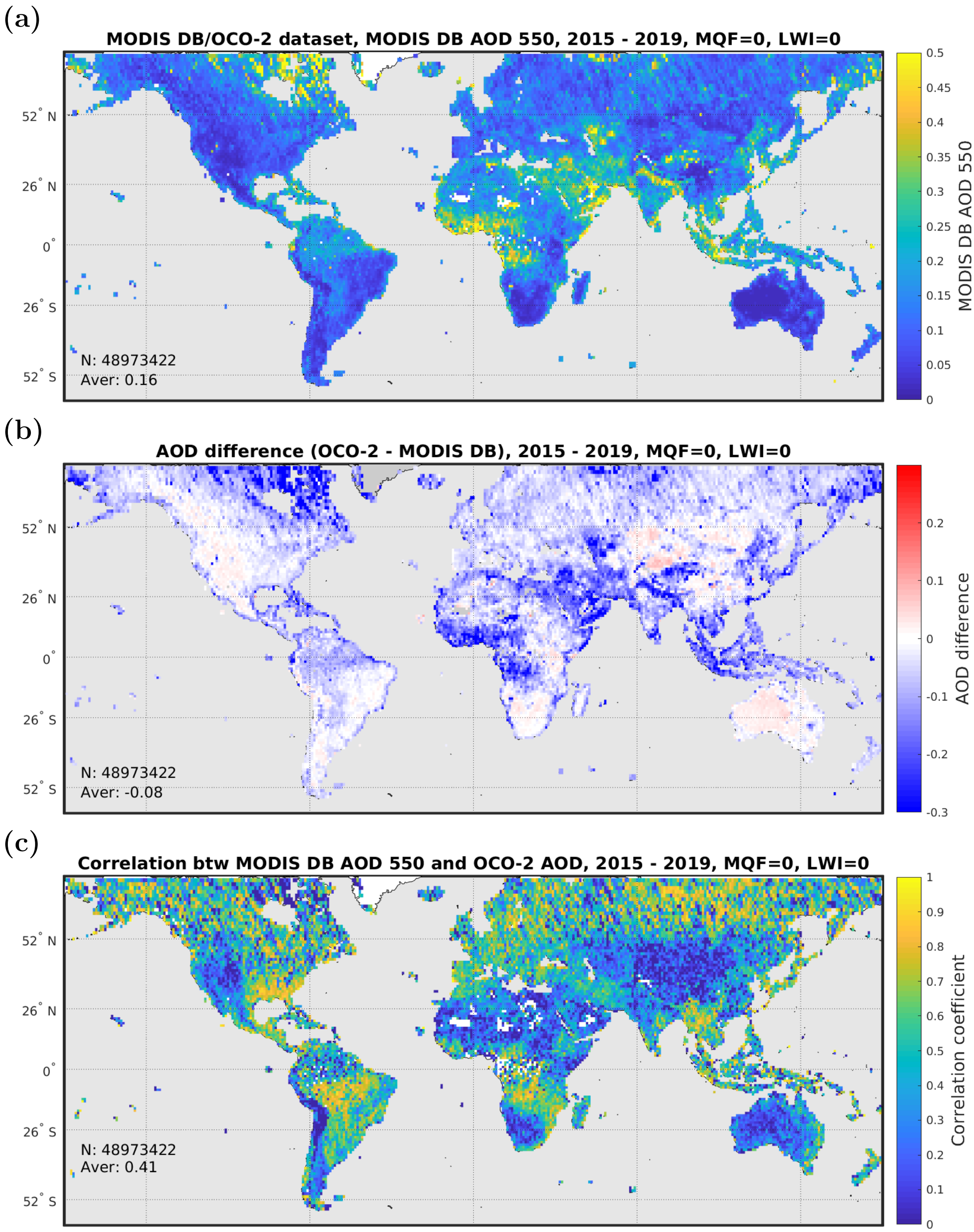


**Figure A2.** Same as Fig. 1, but for MODIS Deep Blue (DB).

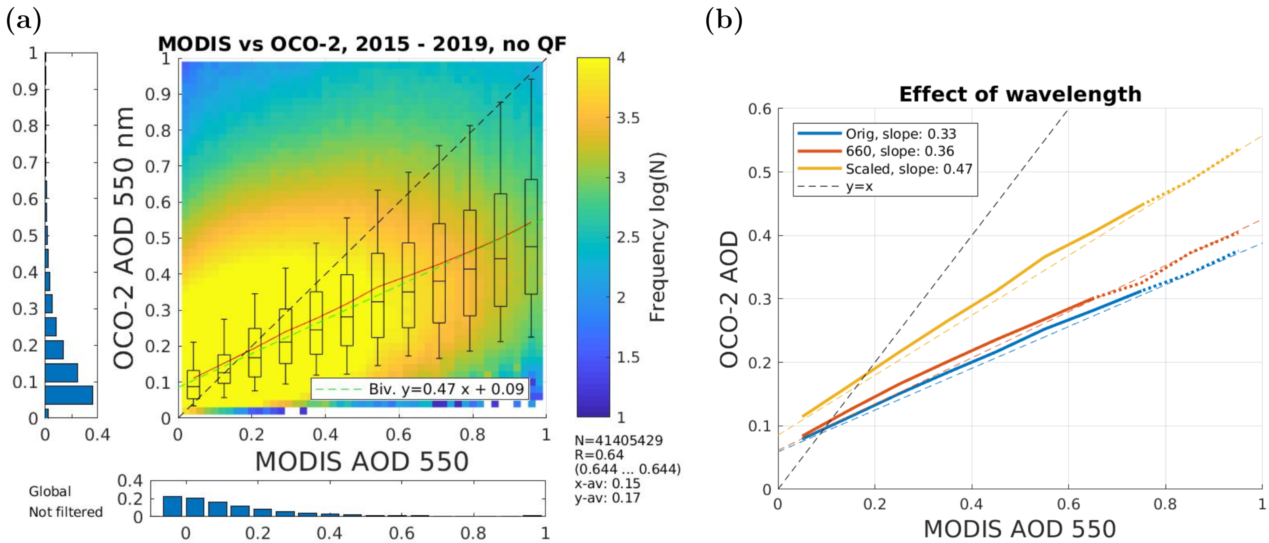


**Figure A3. a)** AOD comparison with OCO-2 AOD scaled from 755 nm to 550 nm using the Angstrom exponent from collocated MERRA-2 data. The red line shows binned mean values, the dashed green line shows bivariate linear fit, the boxes show interquartile range and the whiskers show 9th and 91st percentiles for MODIS AOD bins. **b)** Comparison of OCO-2 AOD against MODIS AOD for three different cases: the original comparison between MODIS AOD at 550 nm and OCO-2 total AOD at 755 nm ('Orig', blue line), MODIS AOD at 660 nm vs OCO-2 AOD at 755 nm ('660', red line); MODIS AOD at 550 nm vs OCO-2 AOD scaled to 550 nm ('scaled', yellow line). Solid lines show bin-averaged OCO-2 AOD (for MODIS AOD bins); the dotted part correspond to bins with less than 1% of all data. Dashed lines show bivariate linear fits. OCO-2 quality filtering has not been applied.

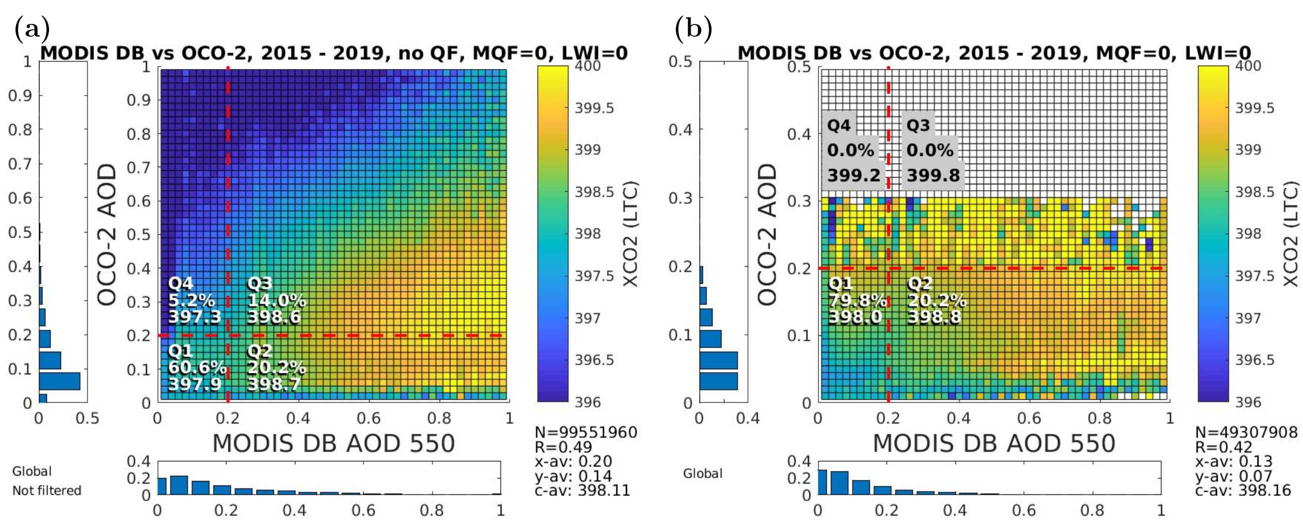


**Figure A4.** Same as Fig. 7, but for MODIS DB.

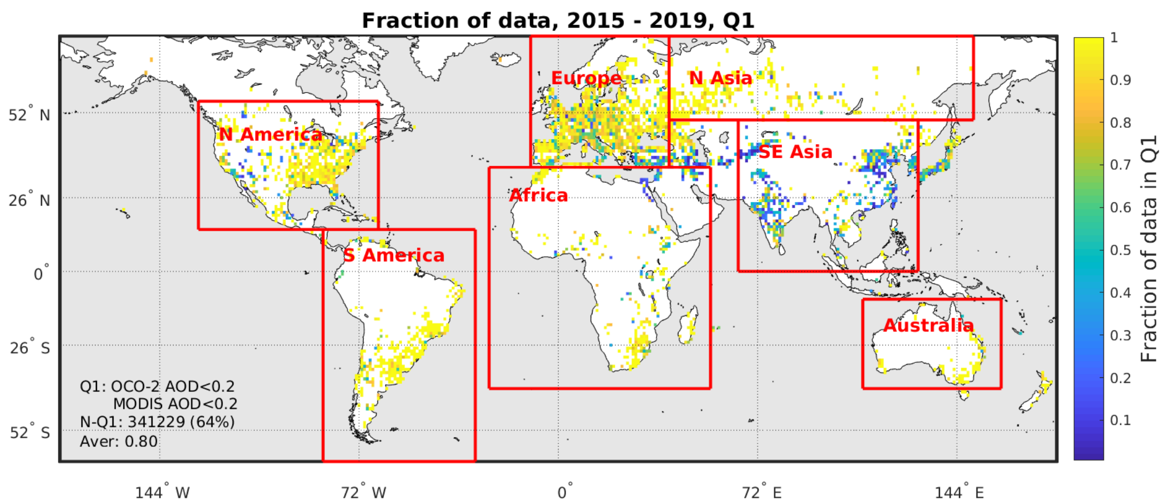


**Figure A5.** Fraction of data in quarter Q1 for urban pixels (areas of dense human habitation using the urban area mask from naturalearth-data.com (NaturalEarth, last access: 22 April 2024). Also shown are the seven geographic areas use in this study.